iScience

Article

The PYRIN domain is required for TLR4-mediated inflammation by PYHIN family members

Graphical abstract

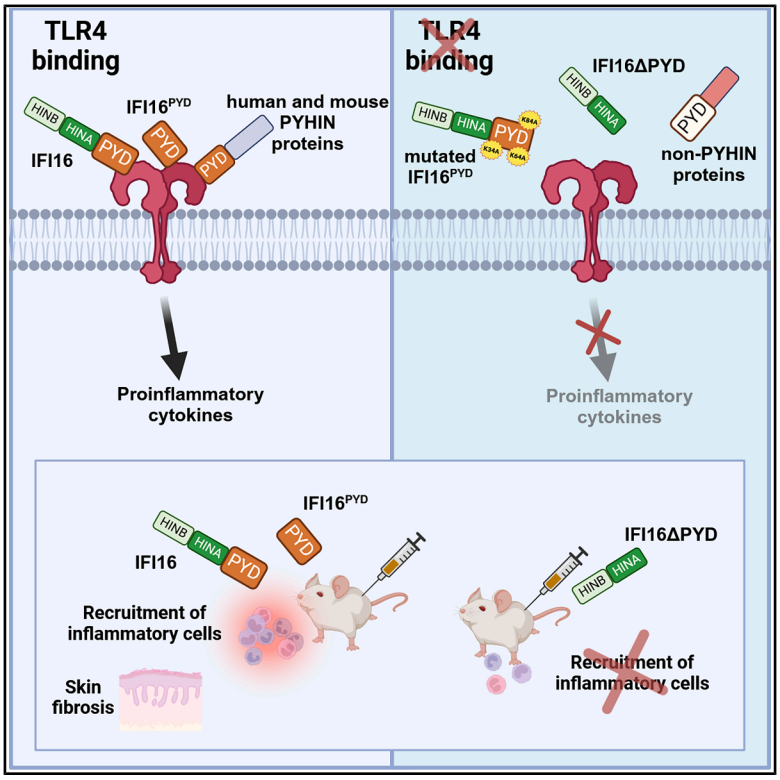

Authors

Andrea Iannucci, Davide Lacarbonara, Valeria Caneparo, ..., Ivan Zanoni, Marisa Gariglio, Marco De Andrea

Correspondence

marco.deandrea@unito.it

In brief

Molecular biology; Immune response; Structural biology

Highlights

- IFI16 acts as a DAMP, triggering TLR4-mediated inflammation *in vitro* and *in vivo*
- The PYD of IFI16 is crucial for binding TLR4 and inducing inflammation
- The inflammatory activity of PYD is unique to human and mouse PYHIN proteins
- The PYD of non-PYHIN proteins do not elicit TLR4 activation

Iannucci et al., 2025, iScience *28*, 112413
May 16, 2025
https://doi.org/10.1016/j.isci.2025.112413

CellPress

iScience

CellPress
OPEN ACCESS

Article

The PYRIN domain is required for TLR4-mediated inflammation by PYHIN family members

Andrea Iannucci,[1,2,7] Davide Lacarbonara,[1,8] Valeria Caneparo,[1] Federica Castiglioni,[1,5] Andrea Butticè,[3] Stefano Raviola,[1,5] Chiara Porta,[1,3] Riccardo Miggiano,[3] Ivan Zanoni,[2,4] Marisa Gariglio,[1,5] and Marco De Andrea[1,6,9,*]

[1]CAAD - Center for Translational Research on Autoimmune and Allergic Disease, University of Eastern Piedmont, 28100 Novara, Italy
[2]Division of Immunology, Harvard Medical School, and Boston Children's Hospital, Boston, MA 02115, USA
[3]Department of Pharmaceutical Sciences, University of Eastern Piedmont, 28100 Novara, Italy
[4]Division of Gastroenterology, Harvard Medical School, and Boston Children's Hospital, Boston, MA 02115, USA
[5]Department of Translational Medicine, University of Eastern Piedmont, 28100 Novara, Italy
[6]Department of Public Health and Pediatric Sciences, University of Turin, Medical School, 10126 Turin, Italy
[7]Present address: Department of Biomedicine and Prevention, University of Rome Tor Vergata, Rome 00133, Italy.
[8]Present address: Department of Pediatrics, Columbia University Vagelos College of Physicians and Surgeons, New York, NY 10032, USA
[9]Lead contact
*Correspondence: marco.deandrea@unito.it
https://doi.org/10.1016/j.isci.2025.112413

SUMMARY

Innate immunity relies on pattern recognition receptors (PRRs) to detect threats, including pathogens and damage-associated molecular patterns (DAMPs) from damaged cells. IFI16 behaves as a DAMP and activates Toll-like receptor 4 (TLR4)-mediated inflammation. Here, we identify the N-terminal PYRIN domain (PYD) of IFI16 as critical for binding TLR4 and triggering inflammation, and we confirm this interaction through *in vitro* and *in vivo* assays. The inflammatory activity of IFI16^{PYD} is unique to human and mouse PYHIN proteins, as PYDs in other proteins, such as NLRP3 or ASC, do not activate TLR4. Disrupting the IFI16-TLR4 interaction prevents pro-inflammatory cytokine production, reducing immune cell recruitment and skin fibrosis in mice. Elevated IFI16 and TLR4 levels in systemic sclerosis patients suggest a role in disease progression. These findings provide insight into DAMP recognition and inflammation propagation, highlighting the IFI16-TLR4 interaction as a potential therapeutic target for sterile inflammatory diseases.

INTRODUCTION

The interferon-inducible protein IFI16 belongs to the HIN200 family of proteins, characterized by one or two consecutive 200-amino acid DNA binding HIN (hematopoietic expression, interferon-inducible nature, and nuclear localization) domains.[1–4] Recently, these proteins have been renamed either PYHIN,[5] because of the presence of one PYRIN domain (PYD) at their N-terminus, or AIM2-like receptors (ALRs) due to their ability to act as a new class of pattern recognition receptors (PRRs).[6,7] PYD, a protein-protein interaction domain belonging to the death domain fold (DDF) superfamily, is known for its oligomerization-dependent signaling function in innate immune responses, particularly in the assembly of inflammasomes.[8,9]

Since its discovery, IFI16 has been linked to a growing range of physiological processes, including cell cycle regulation, tumor suppression, apoptosis, DNA damage signaling, virus detection, and virus restriction.[10–16] IFI16 has also been reported to be aberrantly expressed in chronically inflamed tissues, such as the intestinal epithelium of patients with inflammatory bowel disease (IBD),[17,18] the epidermis and inflammatory dermal infiltrates of patients with systemic lupus erythematosus (SLE),[19,20] salivary epithelial cells and infiltrating lymphocytes in Sjogren's syndrome (SS) patients,[21,22] as well as the skin of individuals with psoriasis (Pso)[23–25] and systemic sclerosis (SSc).[26] Of note, a number of autoimmune conditions, including SSc, RA, SLE, SS, PsA, and IBD, have been associated with the presence of serum circulating IFI16 protein and its specific autoantibodies.[17,19,27–31] Fittingly, we have previously shown that IFI16 is released into the extracellular matrix where it acts as a damage-associated molecular pattern (DAMP), triggering proinflammatory cytokine production in renal and monocytic cell lines through the Toll-like receptor 4 (TLR4) signaling pathway. This effect is induced by IFI16 alone and is further amplified when IFI16 binds one of the microbial agonists of TLR4, the lipopolysaccharide (LPS), via its HINB domain.[32] Despite these insights, it remains to be fully elucidated how IFI16 interacts with TLR4.

This study provides *in vitro* and *in vivo* functional evidence that the proinflammatory activity of IFI16 specifically resides in its N-terminal region and that IFI16^{PYD} is necessary and sufficient for the binding to, and activation of, TLR4. Moreover, we show that the proinflammatory activity of PYD is a shared feature among PYHIN family members, encompassing both human

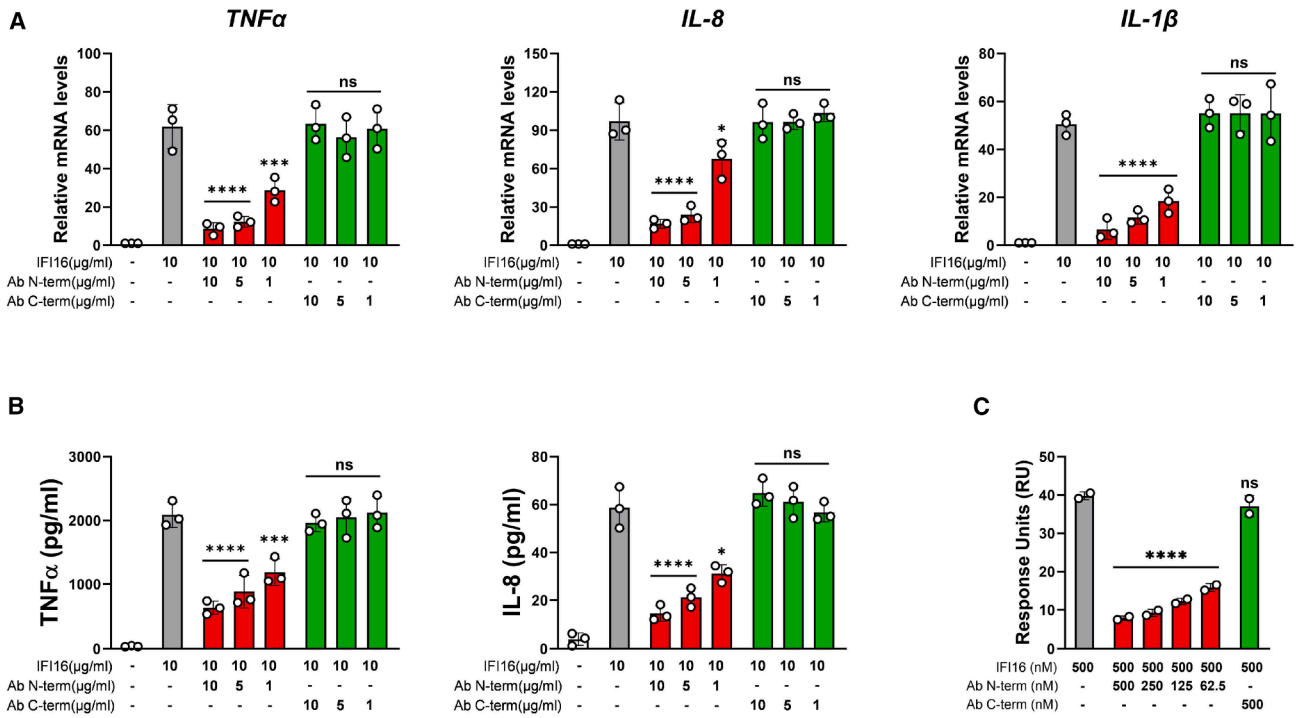

Figure 1. The proinflammatory activity of IFI16 lies within its N-terminal region

(A) qRT-PCR analysis for TNF-α, IL-8, and IL-1β mRNA expression levels in human macrophages stimulated for 24 h with IFI16 alone (10 μg/mL) or pre-incubated for 1 h with the indicated amounts of anti-IFI16 polyclonal antibodies directed against either the N- or C-terminal region of the protein. Values are normalized to GAPDH mRNA and plotted as fold of induction over untreated cells. qRT-PCR data are presented as mean values of biological triplicates. Error bars indicate SEM (*$p < 0.05$, ***$p < 0.001$, ****$p < 0.0001$; one-way ANOVA followed by Dunnett's test).

(B) Protein concentration of TNF-α and IL-8 determined by ELISA in the culture supernatants harvested from human macrophages stimulated for 24 h as described in (A). Data are expressed as mean values ±SEM of three independent experiments (***$p < 0.001$, ****$p < 0.0001$; one-way ANOVA followed by Dunnett's test).

(C) Surface plasmon resonance (SPR) analysis of IFI16 binding to immobilized TLR4. 500 nM of IFI16 diluted in running buffer, alone or pre-incubated for 1 h at RT with increasing concentrations (62.5–500 nM) of the anti-N-term-IFI16 antibody (red bars) or with 500 nM of anti-C-term antibody (green bar), were flowed over a TLR4/MD2-coated chip. Data are representative of two independent experiments, shown as the mean ± SEM (****$p < 0.0001$; one-way ANOVA followed by Dunnett's test).

and mouse genes. We further identify specific amino acids within PYD that are conserved across the PYHIN family, but not found in PYD from other gene families such as the NOD-like receptor (NLR) family pyrin domain-containing protein 3 (NLRP3), which are critically involved in TLR4-mediated proinflammatory activity of these proteins.

RESULTS

The inflammatory activity of the IFI16 protein lies within its N-terminal region

We have previously shown that IFI16 acts as a specific ligand for TLR4.[32] To identify the region within the IFI16 protein responsible for TLR4 activation, we took advantage of antibodies directed against either the N- or C-terminal region of IFI16. Phorbol 12-myristate 13-acetate- (PMA)-differentiated human THP-1 cells (hereafter referred to as human macrophages) were stimulated with 10 μg/mL of full-length IFI16 ($IFI16^{FL}$), either alone or after pre-incubation for 1 h at RT with increasing concentrations of anti-IFI16 antibodies. After 24 h, total RNA was extracted and subjected to qRT-PCR analysis to evaluate the inflammatory response. In agreement with our prior findings,[32] treatment with $IFI16^{FL}$ alone markedly increased the mRNA expression levels of TNF-α, IL-8, and IL-1β compared to untreated cells (61-fold for TNF-α, 97-fold for IL-8, and 50-fold for IL-1β, respectively) (Figure 1A). Interestingly, when IFI16 was pre-incubated with an anti-N-term-IFI16 antibody, there was a noticeable decrease in its ability to upregulate TNF-α, IL-8, and IL-1β gene expression in a concentration-dependent manner. The reduction in transcriptional activation reached approximately 85% at the highest antibody concentration (10 μg/mL). Conversely, the anti-C-term-IFI16 antibody did not affect IFI16-induced cytokine gene expression. This trend aligned with the increased secretion of TNF-α and IL-8 into cell culture supernatants observed after stimulation with $IFI16^{FL}$. Of note, this increase was significantly reduced in a dose-dependent manner with the anti-N-term-IFI16 antibody, in contrast with the lack of any effects observed with the anti-C-term-IFI16 antibody (Figure 1B). The inhibitory activity exerted by the anti-N-term-IFI16 antibody was further confirmed by surface plasmon

resonance (SPR) analysis. IFI16^{FL}, either alone or pre-incubated for 1 h at RT with increasing concentrations of anti-N-term or anti-C-term IFI16 antibody, was flowed over a TLR4/MD2-coated chip. In good agreement with the results obtained with the cellular assay, at concentrations of 500 nM and 62.5 nM, the anti-N-term-IFI16 antibody significantly blocked IFI16 binding to the receptor complex in a concentration-dependent manner, achieving around 75% and 45%, respectively, of binding inhibition compared to controls without antibodies (Figure 1C). As expected, preincubation with the anti-C-term-IFI16 antibody did not impair IFI16 binding to TLR4/MD2 even at the highest concentration.

Collectively, our findings suggest that the N-terminal region of IFI16 is responsible for the recognition and activation of the TLR4/MD2 complex.

The IFI16^{PYD} is involved in TLR4 binding and activation

To precisely map the IFI16 domain responsible for TLR4 binding and activation, we generated a panel of IFI16 recombinant domains spanning the whole protein from the N-terminus to the C-terminus, comprising the PYD, HINA, and HINB domains, alongside truncated versions of IFI16 lacking either the PYD or HINB domain (IFI16ΔPYD or IFI16ΔHINB, respectively) (Figure 2A). Human macrophages were then stimulated with 10 μg/mL of IFI16^{FL} or equimolar concentrations of the IFI16 domains or truncated proteins, followed by total RNA extraction after 24 h for qRT-PCR analysis of pro-inflammatory cytokines. In line with the results shown in Figure 1A and our prior work,[32] TNF-α, IL-8, and IL-1β mRNA expression levels were significantly upregulated upon treatment with IFI16^{FL} or IFI16ΔHINB (Figure 2B). In contrast, stimulation with IFI16ΔPYD led to a substantial reduction in proinflammatory activity, with decreases in mRNA expression levels, compared to untreated cells, ranging from 57- to 10-fold for TNF-α, from 113- to 20-fold for IL-8, and from 48- to 5-fold for IL-1β. Consistently, among the three IFI16 domains, only PYD retained the ability to upregulate the expression levels of TNF-α, IL-8, and IL-1β mRNAs, albeit less effectively than the full-length protein, with mRNA levels increases of 37-fold for TNF-α, 66-fold for IL-8, and 38-fold for IL-1β, compared to untreated cells. To strengthen these findings, we analyzed cytokines secreted in the cell culture supernatant. Accordingly, TNF-α and IL-8 protein levels were significantly higher in supernatants from cells treated with IFI16, IFI16^{PYD}, or IFI16ΔHINB, but not with IFI16ΔPYD or the HINA and HINB domains, compared to untreated cells (Figure 2C). As demonstrated in our earlier findings with IFI16^{FL} protein,[32] the TLR4 dependency of this proinflammatory response was confirmed through its suppression by the TLR4 antagonist CLI-095 (Figure 2C). As shown in Figure S1A, these treatments did not impair cell viability. Similar data were obtained when human primary monocytes or peripheral blood mononuclear cells (PBMCs) were isolated from buffy coats of healthy donors and employed. Under all experimental conditions tested, human cells responded to IFI16^{FL} or IFI16^{PYD} but not to IFI16ΔPYD (Figure S1B). Stimulation of cells with LPS was utilized as a positive control, and while the heterogeneous group of cells present in PBMCs responded more potently to LPS than to IFI16, monocytes showed comparable or higher levels of cytokines than those released upon LPS treatment, suggesting that monocytes are the primary responder to IFI16, while other populations in PBMCs also respond to LPS (Figure S1C).

To assess whether additional domains other than the IFI16^{PYD} could engage TLR4, we conducted SPR analysis. For this purpose, we flowed increasing concentrations of the truncated IFI16^{FL} protein or its distinct domains over a TLR4/MD2-coated sensor chip and assessed the binding affinity and interaction kinetics, which would be indicative of receptor engagement. As shown in Figure 2D and summarized in Table 1, both IFI16ΔHINB and IFI16^{PYD} bound to TLR4/MD2, with affinities (K_D = 7.83*10^{-8} and 4.15*10^{-6}, respectively) comparable to that of IFI16^{FL} (K_D = 1.71*10^{-7}). As expected, no binding to TLR4/MD2 was observed when the IFI16ΔPYD variant was examined. In contrast, the HINA and HINB domains did exhibit biophysical interactions, but their affinity constant values fell within the millimolar range (K_D = 1.57*10^{-4} and 2.98*10^{-4}, respectively), putatively indicating that these interactions were not robust enough to form a stable biological complex.

We next sought to determine whether the PYD could bind to TLR4 on the cell membrane. To this end, human macrophages were treated, or not, with IFI16^{FL}, IFI16^{PYD} or IFI16ΔPYD and co-immunoprecipitation assays were performed where TLR4 and its interacting partners were immunoprecipitated using an anti-TLR4 antibody. The resulting immune complexes were then analyzed by SDS-PAGE followed by immunoblotting for TLR4 or IFI16, using antibodies directed against either the N-term or C-term domains of IFI16. As shown in Figure 2E, the anti-N-term-IFI16 antibody revealed co-immunoprecipitation signals with TLR4 in samples treated with either IFI16^{FL} or IFI16^{PYD}, indicating the capability of IFI16 and its PYD to interact with TLR4 *in vivo*. The specificity of the IFI16^{PYD}-TLR4 interaction was further demonstrated by the lack of signal when the anti-C-term antibody was employed to detect the interaction between TLR4 and the IFI16^{PYD}, or between TLR4 and IFI16ΔPYD, even though the same antibody did recognize co-immunoprecipitated IFI16^{FL}.

Taken together, our findings indicate that the PYD in IFI16 is necessary and sufficient to bind and activate TLR4 signaling and consequent inflammatory responses in human macrophages.

The proinflammatory activity of the PYRIN domain is conserved among PYHIN family members

Next, we asked whether the proinflammatory activity elicited by IFI16^{PYD} could be extended to other members of the PYHIN family, including those from mice, or even to proteins from different gene families harboring PYD, such as NLRP3 and the apoptosis-associated speck-like protein containing a CARD (ASC). To answer this question, we generated recombinant PYDs of representative human [i.e., AIM2 (hAIM2), MNDA, and IFIX] as well as mouse [i.e., Aim2 (mAIM2), Ifi203, and Ifi204] PYHIN proteins, in addition to the human NLRP3 and ASC proteins. Equimolar concentrations of these PYDs were then used to stimulate human macrophages for 24 h, after which total RNAs were extracted and analyzed by qRT-PCR to measure the expression levels of our panel of proinflammatory cytokines. Stimulation with any of the PYD from the PYHIN family (PYHIN-PYD) resulted in a significant increase in TNF-α, IL-8, and IL-1β mRNA expression levels, averaging more than 40-fold

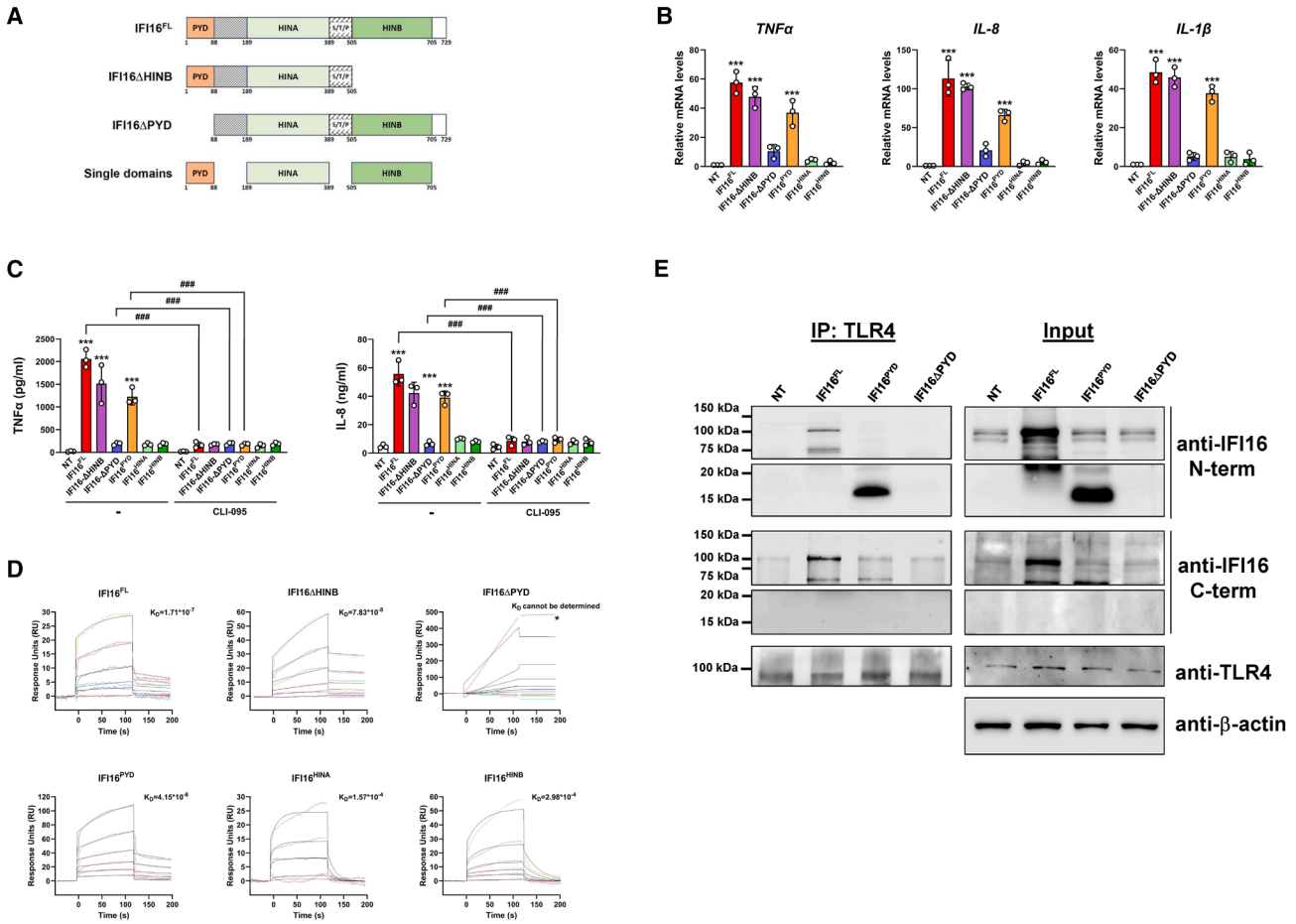

Figure 2. The PYRIN domain of IFI16 is involved in TLR4/MD2 binding and activation

(A) Schematic representation of the full-length IFI16 (IFI16^{FL}), the truncated forms IFI16ΔHINB and IFI16ΔPYD, and the single domains used in this study. Numbers represent the amino acid positions based on the NCBI Reference Sequence GenBank: NP_005522.

(B) qRT-PCR analysis of TNF-α, IL-8, and IL-1β mRNA expression levels in human macrophages stimulated for 24 h with or without the recombinant proteins described in A (111 nM). Values are normalized to GAPDH mRNA and plotted as fold induction over mock-treated cells. qRT-PCR data are presented as mean values ±SEM of biological triplicates (***$p < 0.001$; one-way ANOVA followed by Dunnett's test).

(C) Protein concentration of TNF-α and IL-8 evaluated by ELISA in supernatants derived from human macrophages stimulated for 24 h as described in the legend (B), with or without CLI-095 (TLR4 inhibitor, 5μM). Data are expressed as mean values ±SEM of three independent experiments (***$p < 0.001$; one-way ANOVA followed by Dunnett's test).

(D) SPR analysis of IFI16 mutants or domains binding to immobilized TLR4/MD2. After immobilization of TLR4/MD2 on the CM5 sensor chip surface, increasing concentration of IFI16^{FL}, IFI16ΔHINB, IFI16ΔPYD, IFI16^{PYD}, HINA, or HINB domains (20–800 nM), diluted in running buffer, were injected over the immobilized complex. Data are representative of three different experiments, with the dissociation constant (K_D) value provided where applicable. In the sensogram for IFI16ΔPYD, the asterisk (*) denotes the mass transport effect observed at the highest concentration (2 μM).

(E) Human macrophages were stimulated for 1 h with IFI16^{FL}, IFI16^{PYD}, IFI16ΔPYD, or left untreated (25 μg/mL). Total cellular extracts were then subjected to immunoprecipitation using an anti-TLR4 monoclonal antibody. Immunoprecipitates (left, IP:TLR4) and whole-cell lysates (right, Input) were analyzed by immunoblotting using antibodies against N-term-IFI16, C-term-IFI16 or TLR4. β-actin protein expression served as a protein loading control. Data are representative of three independent experiments with similar results.

upregulation for all the three cytokines compared to untreated cells (Figure 3A). This response was consistent with that observed following exposure to IFI16^{PYD} and was similarly noted with murine proteins. Conversely, stimulation with either NLRP3^{PYD} or ASC^{PYD} did not lead to a significant upregulation of the proinflammatory cytokines when compared to untreated cells. Consistent with these findings, enhanced release of TNF-α and IL-8 was observed in supernatants from cells stimulated with various PYHIN^{PYDs} but not with NLRP3^{PYD} or ASC^{PYD} (Figure 3B). Importantly, the small-molecule TLR4 antagonist CLI-095 effectively blocked the proinflammatory responses promoted by PYHIN^{PYDs}, confirming that their activation occurs through the canonical TLR4/MD2 pathway. Of note, similar results were obtained when murine macrophages (i.e., RAW264.7) were used as target cells. As shown in Figure 3C, PYDs from both human and murine PYHIN family members induced a TLR4-dependent TNF-α release in murine macrophage supernatants, whereas NLRP3^{PYD} or ASC^{PYD} did not.

Table 1. Binding kinetics to TLR4 receptor of IFI16 full length vs. deleted isoforms and single domains

	K_D(M)	Rmax (RU)	tc	Chi^2 (RU^2)	U-value
$IFI16^{FL}$	$1.71*10^{-7}$	9638	$1.33*10^{7}$	1.21	9
IFI16ΔHINB	$7.83*10^{-8}$	54.54	$2.99*10^{6}$	1.47	12
IFI16ΔPYD	undetermined	–	–	–	–
$IFI16^{PYD}$	$4.15*10^{-6}$	64.70	$6.34*10^{17}$	2.73	4
$IFI16^{HINA}$	$1.57*10^{-4}$	1025	$1.49*10^{8}$	0.44	20
$IFI16^{HINB}$	$2.98*10^{-4}$	3213	$2.20*10^{7}$	2.24	15

To further confirm that the proinflammatory activity elicited by $PYHIN^{PYDs}$, unlike those from other gene families, specifically involved the TLR4/MD2 complex, we conducted SPR analyses applying increasing concentrations of $hAIM2^{PYD}$ (human PYHIN), $Ifi203^{PYD}$ (murine PYHIN), or $NRLP3^{PYD}$ (non-PYHIN) on a sensor chip coated with TLR4/MD2. As expected, both $hAIM2^{PYD}$ and $Ifi203^{PYD}$ showed high affinity binding to TLR4/MD2, with a K_D comparable to that of $IFI16^{PYD}$ ($3.48*10^{-6}$ for hAIM2 and $6.06*10^{-6}$ for Ifi203 vs. $4.15*10^{-6}$ for IFI16). In contrast, $NLRP3^{PYD}$ interacted with TLR4/MD2 with a significantly higher K_D ($1.09*10^{-4}$), suggesting a lesser tendency toward complex formation compared to hAIM2 and Ifi203 PYDs (Figure 3D and Table 2).

Collectively, these findings demonstrate that $PYHIN^{PYDs}$ specifically retain the ability to induce a TLR4-mediated proinflammatory phenotype in target cells. Remarkably, this function is consistent across PYHIN proteins of both human and mouse origin, implying the existence of conserved mechanisms of interaction between these two species.

Three amino acids located within the $IFI16^{PYD}$ are critically involved in its TLR4-mediated proinflammatory activity

Having established the TLR4-dependent proinflammatory activity of $PYHIN^{PYDs}$, we selected $IFI16^{PYD}$ as a representative member of the PYHIN family to assess the specificity of its interaction with TLR4 at the structural level. By means of the Robetta software,[33] we predicted its 3D structure (Figure 4A) and used it to perform a molecular docking study with the extracellular domain of TLR4 (PDB:3FXI, Figure 4B) through High Ambiguity Driven protein-protein DOCKing (HADDOCK) software.[34] In parallel, we aligned the sequence of $PYHIN^{PYDs}$ with those from NLRP3 and ASC proteins to identify PYHIN-specific amino acids sharing similar chemical properties (Figure 4C). This process, which merged sequence alignment with molecular docking insights, focused on: (1) bond lengths shorter than 3 Å, (2) the chemical properties of the amino acids in question, and (3) unique characteristics of $PYHIN^{PYDs}$. This comprehensive analysis allowed us to identify three residues in $IFI16^{PYD}$ —specifically, Lys34, Lys64, and Lys86—potentially involved in the interaction with TLR4 (Figure 4C, light blue arrows; Figure 4D). Interestingly, these residues are either conserved or maintain similar properties across PYHIN family members of both human and mouse origin (Figure S2). Furthermore, superimposing the 3D structure of $IFI16^{PYD}$ with those of $NLRP3^{PYD}$ and ASC^{PYD} using PyMOL software revealed that these critical amino acids are replaced by residues with different chemical properties and orientations in non-PYHIN family members, likely preventing binding to TLR4 (Figure S3). This effect appears to be further exacerbated by the presence of an extended loop in the $NLRP3^{PYD}$ and ASC^{PYD} structures, which may interfere with receptor binding due to steric hindrance. Specifically, these loop moieties occupy the region in $IFI16^{PYD}$ meant for TLR4 engagement through electrostatic interaction involving both Lys34 and Lys64.

To assess the biological relevance of these predictions and confirm the involvement of these residues in TLR4 activation, we created alanine substitutions at the identified polar residues through site-directed mutagenesis, giving rise to the IFI16 mutants K34A and K86A (Figure 5A). In addition, to reduce non-specific interactions potentially caused by the methyl group of alanine due to steric hindrance, thus enhancing TLR4 interaction, we replaced Lys64 with glycine, obtaining the K64G mutant. Finally, to test the specificity of $PYHIN^{PYDs}$ and TLR4 interaction, we mutated the conserved Ile17 residue within PYD, not involved in receptor binding, to alanine, creating the I17A mutant (Figure 5A). All these IFI16 mutants, including the $IFI16^{FL}$ and $IFI16^{PYD}$ triple mutants K34A/K64G/K86A ($IFI16^{FL-TM}$ and $IFI16^{PYD-TM}$, respectively), were then used to stimulate human macrophages for 24 h at equimolar concentrations alongside $IFI16^{FL}$. We observed a significant decrease in TNF-α release in the culture supernatants from cells treated with these mutants, except for I17A (Figure 5B). Specifically, TNF-α secretion was diminished by approximately 95%, 75%, and 90% for the K34A, K64G, and K86A $IFI16^{FL}$ single mutants, respectively, compared to the $IFI16^{FL}$ wild-type protein, demonstrating their direct involvement in IFI16 binding to TLR4. Similarly, both $IFI16^{FL-TM}$ and $IFI16^{PYD-TM}$ displayed a significant decrease in TNF-α production (∼85% and ∼94% for $IFI16^{FL-TM}$ and $IFI16^{PYD-TM}$, respectively).

The ability of each mutant to physically interact with TLR4 was assessed through SPR analysis. This consisted in flowing increasing concentrations of the IFI16 mutants or the full-length protein over the aforementioned TLR4/MD2-coated sensor chip. As depicted in Figure 5C, single mutations at key amino acids previously identified as essential for TLR4 interaction, namely K34A, K64G, and K86A, curbed binding to TLR4/MD2, as judged by increased K_D values and unreliable fitting parameters (Table 3). This decreased binding affinity led to impaired interaction kinetics, with sensorgrams for the mutants failing to achieve the saturation levels indicative of a stable interaction (Figure 5C). A similar outcome was observed for the $IFI16^{FL-TM}$, while the I17A mutant maintained high-affinity binding to the TLR4/MD2 complex ($K_D = 1.75*10^{-7}$), comparable to the affinity seen with the wild-type $IFI16^{FL}$ protein ($K_D = 1.71*10^{-7}$).

Altogether, these findings confirm the high-affinity interaction between $PYHIN^{PYD}$ and TLR4 and pinpoint specific amino acids in $IFI16^{PYD}$ crucial for this interaction.

The IFI16 PYD contributes to inflammation *in vivo*

IFI16 is a human protein and has no clear-defined ortholog in mice.[7] However, having shown that IFI16 can also elicit an inflammatory response from murine macrophages (Figure 3C),

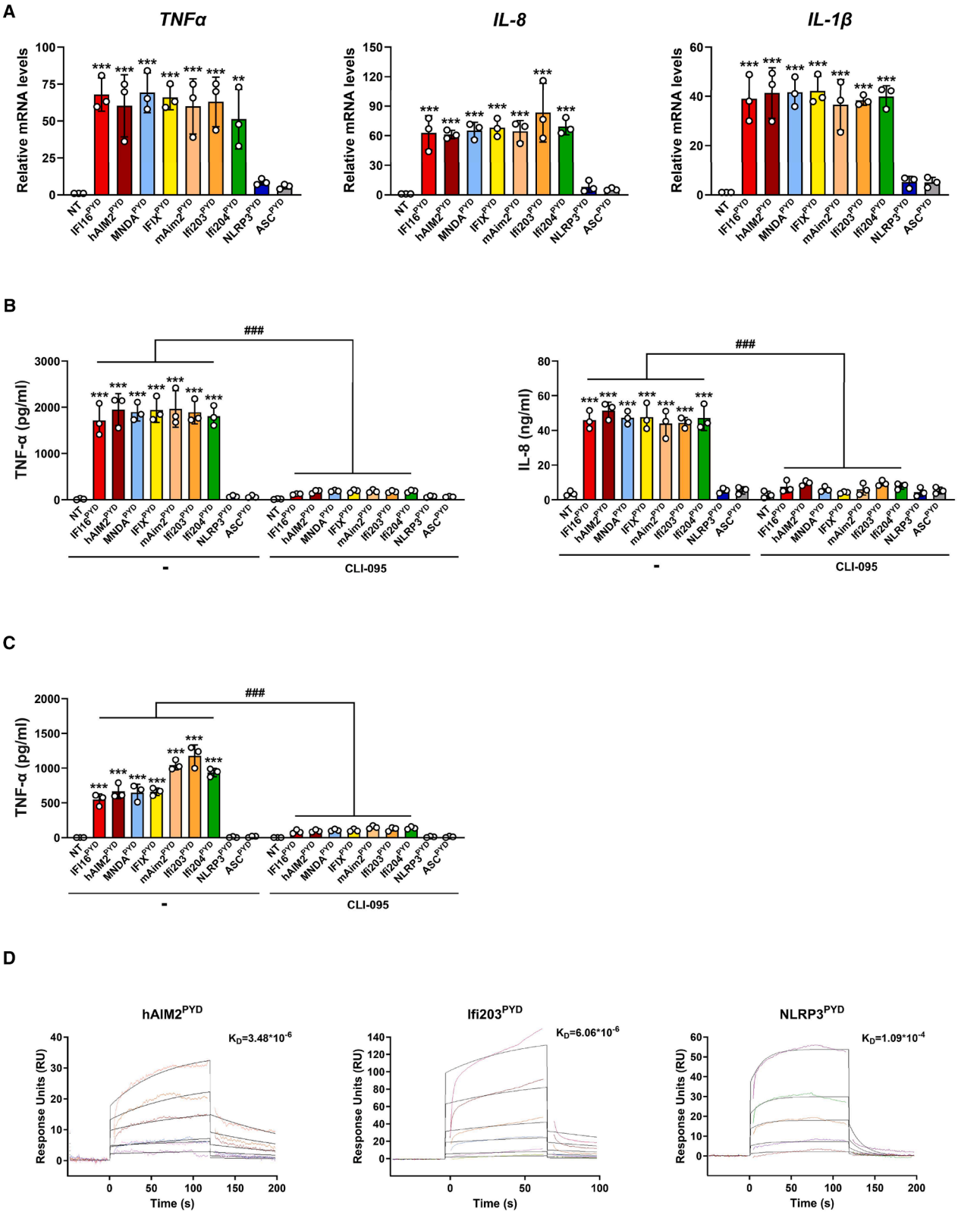

(legend on next page)

Table 2. Binding kinetics of various PYDs to TLR4 receptor

	K_D(M)	Rmax (RU)	tc	Chi^2 (RU^2)	U-value
$hAIM2^{PYD}$	$3.48*10^{-6}$	16.33	$2.480*10^{19}$	0.19	5
$Ifi203^{PYD}$	$6.06*10^{-6}$	57.28	$2.216*10^{8}$	8.61	33
$NLRP3^{PYD}$	$1.09*10^{-4}$	317.10	$8.92*10^{8}$	0.855	15

we tested whether IFI16 retained its inflammatory activity in mice *in vivo*. To this end, we first intraperitoneally injected $IFI16^{FL}$, $IFI16^{PYD}$, IFI16ΔPYD, or vehicle control in wild-type C56BL/6 mice. After 24 h, mice were sacrificed, and cells recovered from the peritoneal cavity were analyzed by fluorescence-activated cell sorting (FACS) to evaluate both neutrophil recruitment and macrophage activation (Figure 6A). As shown in Figure 6B, both $IFI16^{FL}$ and $IFI16^{PYD}$ significantly increased the number of peritoneal neutrophils (CD11b+Ly6G + Ly6C- cells) when compared to those depicted in untreated animals. Conversely, the number of peritoneal neutrophils recruited following IFI16ΔPYD treatment was significantly lower than that observed with $IFI16^{FL}$ or $IFI16^{PYD}$. Consistently, also the number of peritoneal macrophages displaying the standard activation markers, e.g., MHC class II (I-A/I-E) and CD86, were significantly increased in mice treated with either $IFI16^{FL}$ or $IFI16^{PYD}$ when compared to both untreated mice and those treated with IFI16ΔPYD (Figure 6C). Overall, these findings demonstrate that IFI16, through its PYD domain, can elicit an inflammatory response *in vivo*.

Next, considering the aberrant expression and extracellular release of IFI16 in many inflammatory skin disease, and the mounting evidence suggesting that activation of the DAMP-TLR4 axis drives persistent fibrinogenesis,[35,36] we injected the $IFI16^{FL}$ protein intradermally in mice to see if we could mimic the fibrotic phenotype executed by intradermal administration of bleomycin, a well-known experimental mouse model of skin fibrosis.[37] The lesional skin harvested after 6 weeks of continuous every-other-day treatment with $IFI16^{FL}$, revealed a significant enhancement of both dermal thickness and collagen deposition, as determined by Masson's trichrome staining, very much resembling that observed upon bleomycin injection (∼1.6-fold for both, compared to vehicle-treated animals; Figure 6D). In addition, the number of mast cells was also quantified in serial sections by toluidine blue staining. Consistently, mast cells recruitment was found increased in the skin of mice injected with $IFI16^{FL}$ when compared to vehicle-treated animals (∼5.9-fold) (Figure 6E). Notably, this enhancement was significantly higher than that observed in bleomycin-treated mice (∼3.3-fold compared to vehicle-treated mice).

Finally, we analyzed multiple transcriptome datasets of human patients with SSc (GSE9285, GSE32413, and GSE45485; https://www.ncbi.nlm.nih.gov/geo/ [38]) and found that the *IFI16* mRNA levels were significantly elevated in skin biopsies characterized by an inflammatory transcriptional program ($p < 0.0001$, compared to healthy controls and to the limited or diffuse proliferative intrinsic subsets) (Figure S4A). Consistently, *IFI16 mRNA* levels correlated with both *TLR4* and *TNFA* mRNA levels in the same samples ($r = 0.2397$, $p < 0.01$ and $r = 0.1891$, $p < 0.05$, respectively, Pearson's correlation) (Figure S4B).

Overall, these findings provide compelling evidence that $IFI16^{FL}$ triggers inflammation *in vivo* in mice and that IFI16 levels correlate with inflammation in humans.

DISCUSSION

In our work, we systematically analyze the domains of IFI16 that allow the interaction with TLR4, driving the production of pro-inflammatory response in human macrophages. Through functional cellular assays on target cells and SPR experiments, we identify that the N-terminal region of IFI16 is required for TLR4 binding and to drive inflammation. Furthermore, by examining a series of IFI16 recombinant domains covering the entire protein from its N-terminus to the C-terminus, comprising the PYD, HINA, or HINB domains, as well as the truncated IFI16ΔPYD and IFI16ΔHINB isoforms, we demonstrate that PYD is necessary and sufficient for TLR4 binding and activation in human macrophages. These results are in good agreement with our previous data showing that IFI16ΔHINB isoform is still able to drive inflammation despite the binding with LPS being prevented.[32] Together, these findings suggest that IFI16 exerts a dual mode of immune regulation: while the HINB domain facilitates LPS binding and amplifies TLR4-driven responses, the PYD domain is independently capable of engaging TLR4, even under LPS-free conditions. This highlights the structural and functional versatility of IFI16 in modulating inflammatory pathways and further supports its role as a multifunctional regulator of innate immunity.

Although IFI16 is predominantly nuclear under physiological conditions, increasing evidence suggests that it can be actively released into the extracellular space under inflammatory conditions. Notably, IFI16 has been detected in the serum of patients with autoimmune diseases at physiologically relevant concentrations, supporting its potential role as an extracellular modulator of immune responses.[21,22] While we did not directly quantify IFI16 release in cell culture supernatants in this study, previous

Figure 3. The proinflammatory activity of the PYRIN domain is conserved among PYHIN family members and across species

Equimolar concentrations (111 nM) of the PYDs from various human and mouse family members, as well as from the unrelated NLRP3 and ASC proteins, were used to stimulate human (A and B) or mouse (C) macrophages for 24 h, with or without CLI-095 (TLR4 inhibitor, 5 μM). (A) qRT-PCR analysis of TNF-α, IL-8, and IL-1β mRNA expression levels in human macrophages stimulated for 24 h. Values are normalized to GAPDH mRNA and plotted as fold induction over untreated cells. qRT-PCR data are presented as mean values ±SEM of biological triplicates (***$p < 0.001$, **$p < 0.01$; one-way ANOVA followed by Dunnett's test). (B and C) Protein concentration of TNF-α and IL-8 in the supernatants were evaluated by ELISA. Data are representative of three independent experiments, shown as the mean ± SEM (***$p < 0.001$, ###$p < 0.001$; one-way ANOVA followed by Dunnett's test).

(D) SPR analysis showing the binding of various PYDs to TLR4/MD2. The TLR4/MD2 complex was immobilized on a CM5 sensor chip surface, followed by the injection of increasing concentrations of the indicated PYDs (20–800 nM) in running buffer. Data are representative of three different experiments, and for each analysis the dissociation constant (K_D) value is shown.

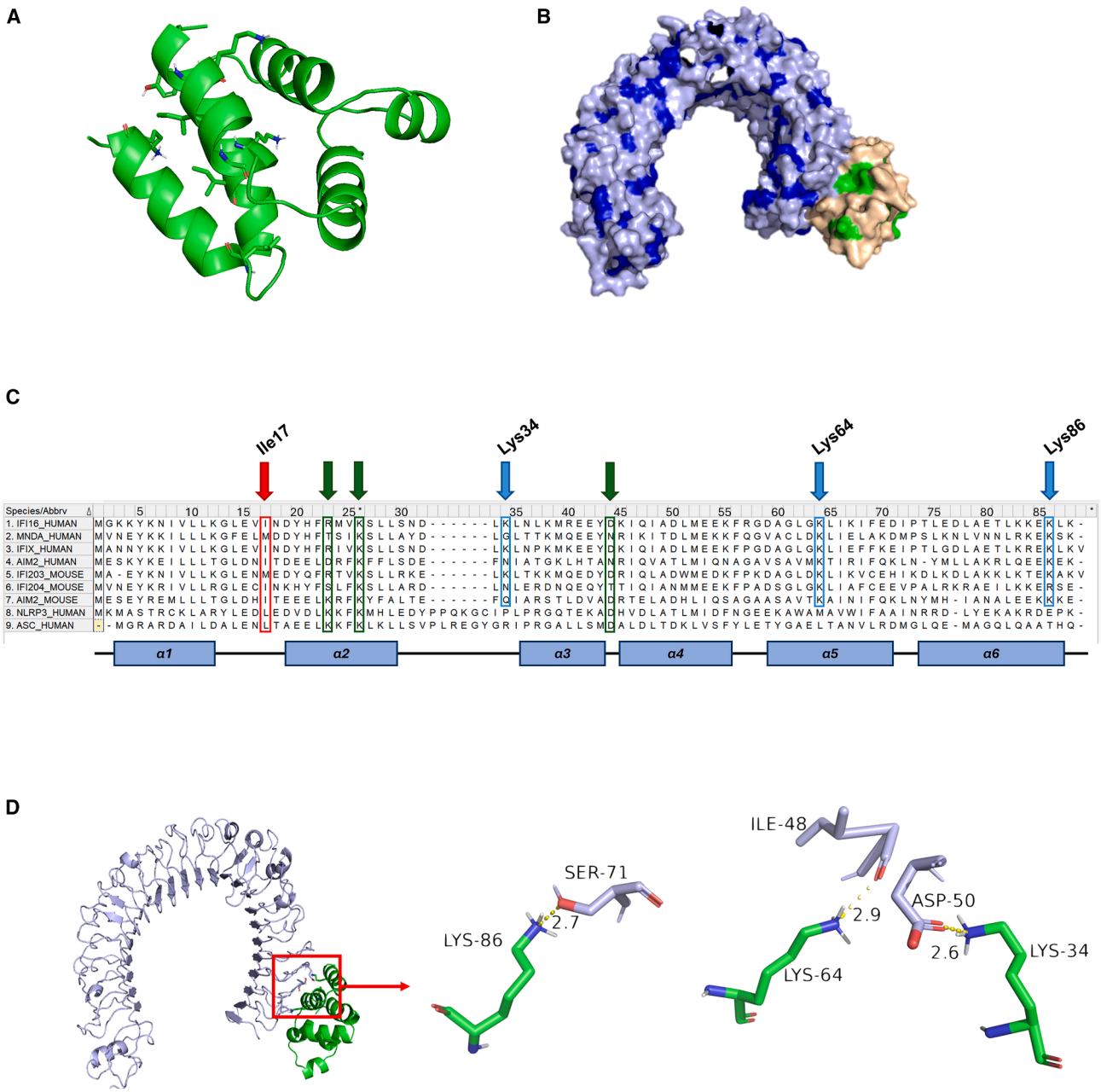

Figure 4. Structural analysis of the interaction moiety between the IFI16^{PYD} and the TLR4/MD2 complex

(A) Predicted 3D structure of the IFI16^{PYD} using the Robetta software.[33]

(B) Molecular docking analysis of the IFI16^{PYD} (green) and the extracellular portion of TLR4 (blue, PDB:3FXI) using High Ambiguity Driven protein-protein DOCKing software.[34]

(C) Alignment of the primary sequence of PYHIN^{PYDs} along with those of NLRP3 and ASC performed using MEGAX and ClustalW algorithm to identify PYHIN-specific amino acids with similar chemical properties. Green arrows identify amino acids conserved across the different proteins, whereas light blue arrows identify amino acids that are conserved only across the PYHIN family members, which were used in mutagenesis experiments (see Figure 5). The red arrow identifies an amino acid conserved in all the proteins, which was mutated and used as control. The six α helices of the PYDs with known structures are also indicated.

(D) Identification of the IFI16^{PYD} residues (green) potentially involved in the interaction with TLR4 (Lys34, Lys64, and Lys86) obtained by integrating the alignment and molecular docking information.

findings indicate that extracellular IFI16 can elicit cytokine release from immune cells, reinforcing the relevance of the concentrations used in our experiments.[32]

In keeping with TLR4 being the receptor that drives the response to IFI16^{PYD}, the addition of the TLR4 antagonist CLI-095[39,40] abolishes the proinflammatory activity of IFI16^{PYD}. We also show

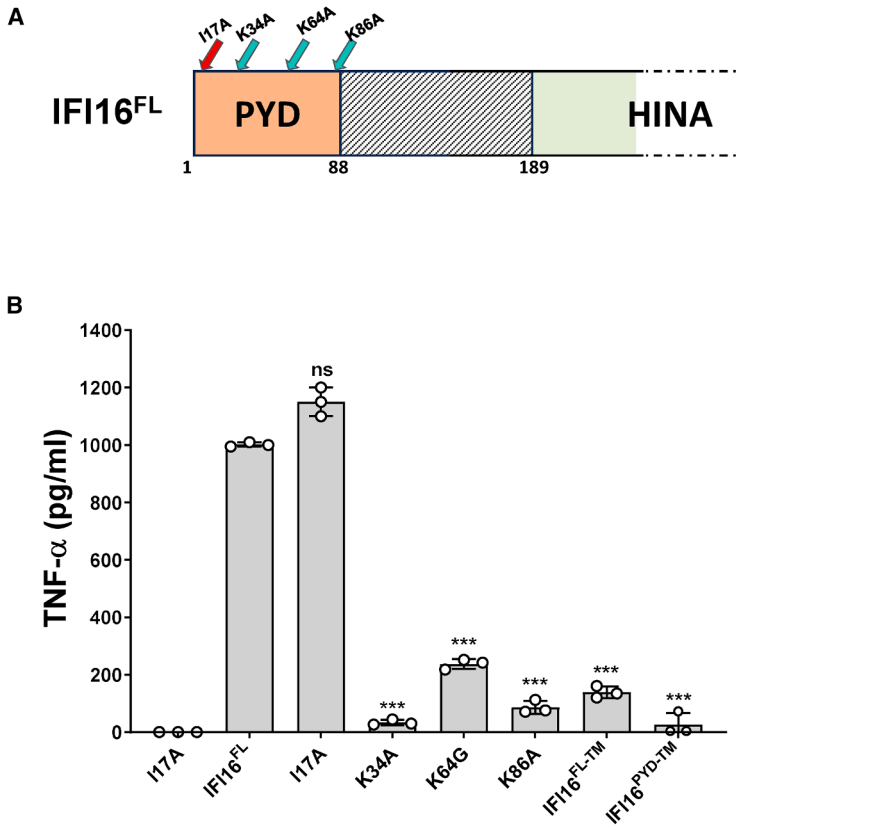

Figure 5. Three amino acids located within the IFI16^{PYD} are critically involved in its TLR4-mediated proinflammatory activity

(A) Schematic representation of the polar residues identified in Figures 4E and 4F, highlighting their positions within the IFI16^{PYD} and the specific amino acid substitutions used in the mutagenesis experiments.

(B) Human macrophages were stimulated for 24 h with equimolar concentrations (111 nM) of the IFI16 mutants described in (A) and the IFI16^{PYD-TM}, alongside the wild type IFI16^{FL}. The levels of TNF-α released in the culture supernatants were measured by ELISA. Data are representative of three independent experiments, shown as the mean ± SEM (*$p < 0.05$, **$p < 0.01$, ***$p < 0.001$; one-way ANOVA followed by Dunnett's test).

(C) SPR analysis assessing the binding of IFI16^{FL} and its mutants to immobilized TLR4/MD2 on a CM5 sensor chip. Increasing concentration of IFI16^{FL} or the mutants (20–800 nM), diluted in running buffer, were flowed over the immobilized complex. Data are representative of three different experiments, and for each analysis the dissociation constant (K_D) value is shown.

that this inflammatory activity is not unique to IFI16 as it is shared among PYHIN family members across humans and mice. Specifically, human AIM2, IFIX and, MNDA, as well as mouse Aim2, Ifi204, and Ifi203—the latter sharing the highest homology to IFI16 in its N-terminus—are equally able to induce TLR4-dependent transcription, leading to the secretion of inflammatory cytokines. This activity is not species-specific since both mouse and human macrophages show similar reactivity to PYDs from either species. Further supporting this observation, SPR analysis reveals that both human AIM2 and mouse Ifi203 PYDs bind to TLR4/MD2 with affinity and kinetics very much resembling those seen with IFI16^{PYD} (Table 2). This evidence points to a conserved mechanism of PYD-mediated TLR4 activation, likely due to the substantial homology (65%)[41] between human and murine TLR4, and highlights the cross-species conservation of PYHIN PYDs,[42] uncovering a shared evolutionary pathway.

PYD, originally identified in the pyrin protein, also known as Marenostrin,[43] belongs to the DDF superfamily.[44] It comprises six anti-parallel alpha helices arranged in a Greek key structure,[45] tightly packed around a hydrophobic core with a highly charged surface. This distinctive configuration is found at the amino terminal end of more than 20 human proteins involved in apoptotic and inflammatory signaling pathways,[46,47] including NLRs, ASC, pyrin itself, and ALRs. These proteins act as intracellular adaptor proteins, negative regulators, or PRRs involved in inflammatory cascades.[48–50] A unifying trait among them is a highly bipolar electrostatic surface patch distribution on the PYD surface, which allows specific PYD–PYD interactions

Table 3. Binding kinetics to TLR4 receptor of IFI16^{FL}-PYD mutants

	K_D(M)	Rmax (RU)	Tc	Chi^2 (RU^2)	U-value
IFI16^{FL}	1.71*10^{-7}	9638	1.33*10^{7}	1.21	9
IFI16^{FL}-K34A	4.82*10^{-5}	4568	3.16*10^{6}	17	20
IFI16^{FL}-K64G	undetermined	–	–	–	–
IFI16^{FL}-K86A	8.42*10^{-5}	3233	1.74*10^{8}	94	20
IFI16^{FL-TM}	undetermined	–	–	–	–
IFI16^{FL}-I17A	1.75*10^{-7}	38.14	3.55*10^{13}	3.39	4

between proteins.[46] The activation and assembly of PYD-dependent inflammasome complexes are triggered by PAMPs engaging with specific PRRs, a process that initiates antimicrobial and inflammatory responses.[51] On the other hand, emerging evidence also indicates that DAMPs, produced by stressed or damaged cells,[52] can similarly activate PYD-dependent inflammatory pathways associated with sterile inflammation.

The above mechanistic insight provides the rationale for understanding the pathological consequences of inflammasome dysregulation, which has been implicated in a variety of autoimmune and autoinflammatory diseases.[53] A paradigmatic example is represented by the familial Mediterranean fever (FMF), the most prevalent systemic autoinflammatory disease (SAID),[54,55] whose underlying mechanisms stem from the aberrant interactions between mutant pyrin and chaperones molecules, leading to a pathological inflammasome-dependent release of IL-1β.[56] Likewise, the dysregulated expression of the PYD-containing NLRP3 protein has been associated with a group of autosomal dominant diseases known as NLRP3-AID

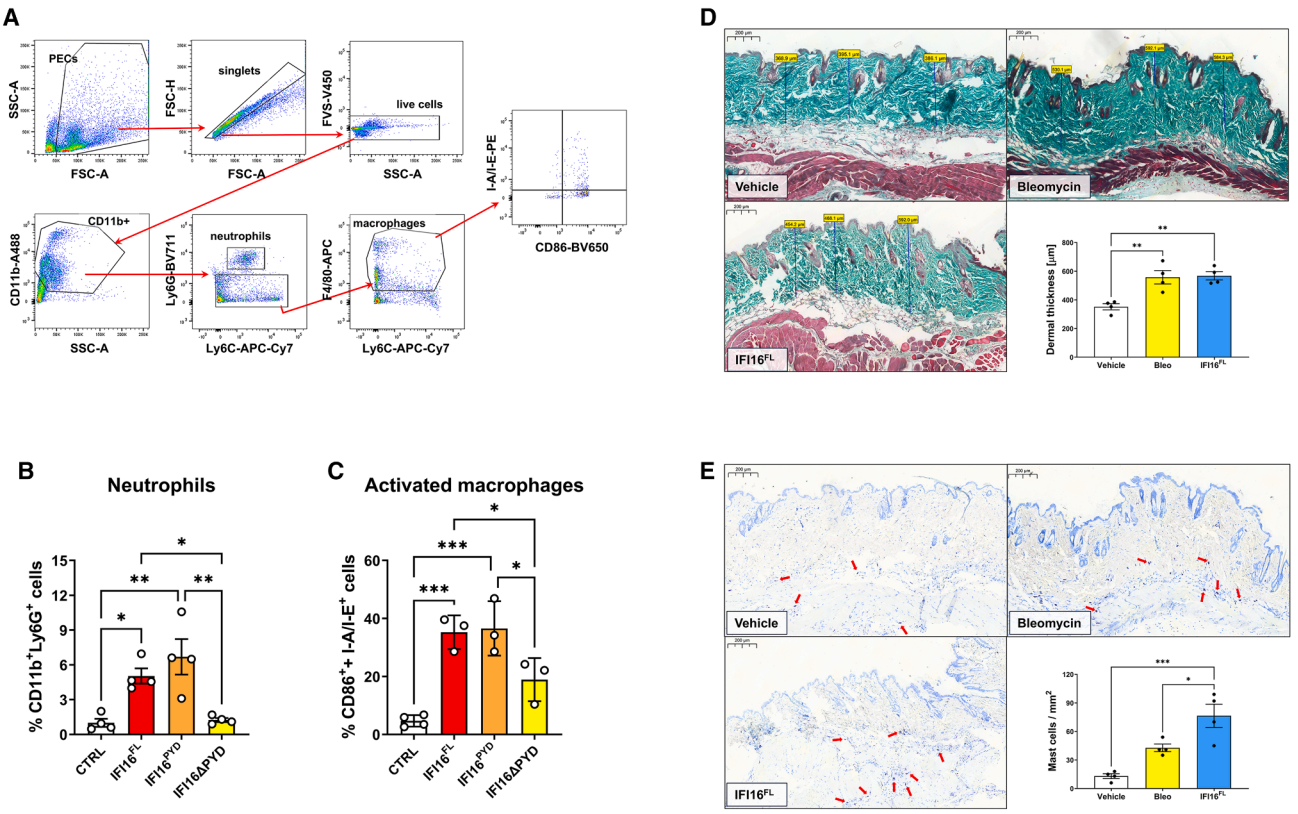

Figure 6. IFI16 induces neutrophil recruitment, macrophage activation and fibrosis *in vivo*

(A–C) C57BL/6J mice were i.p. injected with 5 mg/kg IFI16^{FL}, 5 mg/kg IFI16^{PYD}, 5 mg/kg IFI16ΔPYD or vehicle as control. After 24h peritoneal exudated cells (PECs) were harvested and neutrophil recruitment and macrophage activation were analyzed by FACS. (A) Representative FACS plots showing the gating strategy for FACS analysis of neutrophils and inflammatory activated macrophages in PEC samples. The bar graphs depict the frequency of (B) neutrophils (CD11b+Ly6G + Ly6C- cells) among total live PECs and (C) macrophages (CD11b+F4/80+Ly6G-Ly6C- cells) expressing the activation markers I-A/I-E (MHC II) and CD86 among total macrophages (*$p < 0.05$, **$p < 0.01$ by two-tailed one-way ANOVA).

(D and E) C57BL/6J mice received every other day for 6 weeks s.c. injections of PBS (vehicle), bleomycin (Bleo, 0.1 U/ml), or IFI16^{FL} (50 μg). Mice were sacrificed at day 22, and skin was harvested for analysis. (D) Dermal collagen deposition was assessed by Masson's trichrome staining and analyzed for dermal thickness, as indicated by the lines in the representative photomicrographs on the left (scale bar: 200 μm). Results are shown in the right histograms where each dot indicate the mean of three different measurements per skin sample. Error bars indicate SEM (*$p < 0.05$, **$p < 0.01$, ***$p < 0.001$; one-way ANOVA followed by Dunnett's test; $n = 4$ per group). (E) Mast cells recruitment was assessed by toluidine blue staining, as shown in the representative photomicrographs on the left (scale bar: 200 μm) where black arrows indicate representative mast cells. Results are shown in the right histograms as mean values of two different measurements per skin sample. Error bars indicate SEM (*$p < 0.05$, **$p < 0.01$, ***$p < 0.001$; one-way ANOVA followed by Dunnett's test; $n = 4$ per group).

or cryopyrin-associated periodic syndromes (CAPS),[57–59] characterized by uncontrolled activation of caspase-1 and excessive pro-IL-1β and pro-IL-18 cleavage into their biologically active forms. Furthermore, supporting our hypothesis that extracellular PYD-containing proteins, acting as DAMPs, contribute to the development of inflammatory processes, aggregates containing both ASC and NLPR3 have been found in the blood from patients with chronic inflammatory diseases and acknowledged as significant circulating biomarkers of inflammation.[60–63] However, despite the extensive data available, the specific signaling pathways underlying the inflammatory activities of these PYD-containing DAMPs remain largely unknown.

In this study, we provide compelling evidence that the PYD from both human and mouse PYHIN proteins acts as a direct initiator of inflammation in macrophages via TLR4, which is consistent with the high degree of similarity observed between human and murine TLR4 proteins.

Another important finding from our study is the distinct pro-inflammatory role played by PYDs from various PYHIN family members. This feature does not seem to be shared by other PYD-harboring proteins as recombinant PYDs from NLRP3 and ASC fail to elicit pro-inflammatory activity when used to treat human or murine macrophages.

Our study also unveils previously unrecognized 3D structures of the IFI16^{PYD}, detailed through molecular docking analysis incorporating the extracellular portion of TLR4 as well. This analysis, along with sequence alignments of the PYDs from PYHIN members, such as human MNDA, human and mouse AIM2, human IFIX, and mouse Ifi203 and Ifi204, and non-PYHIN proteins like human NLRP3 and ASC, tells us that IFI16^{PYD} uniquely carries three residues likely crucial for interactions with TLR4 (Lys34, Lys64, and Lys86). Interestingly, these residues are conserved among PYHIN family proteins, while in non-PYHIN members (e.g., human NLRP3 and ASC) they are replaced by other amino acids with different chemical properties or orientations, expected to impede TLR4/MD2 interactions. Consistently, the sequence alignment of IFI16^{PYD} with the PYDs of other murine PYHIN family members supports the hypothesis of a shared "inflammatory pattern" in both human and mouse PYHIN proteins (Figure S2), further reinforcing the evolutionary conservation of this immune mechanism. Furthermore, the comparison of the projected 3D structure of IFI16^{PYD} with those of NLRP3^{PYD} and ASC^{PYD} shows that these latter are characterized by extended loops located precisely where the Lys34 and Lys64 residues of IFI16^{PYD} are supposed to engage with TLR4. These structural/conformational changes may then interfere with TLR4 binding due to steric hindrance. In agreement with these observations, we show that mutating any of these identified residues in the PYHIN domain of the IFI16^{FL} significantly reduces its proinflammatory activity, as judged by reduced TNF-α production in macrophages exposed to these recombinant proteins. Similarly, human macrophages treated with either the IFI16^{FL} or IFI16^{PYD} triple mutants (K34A/K64G/K86A; IFI16^{FL-TM} and IFI16^{PYD-TM}) exhibited reduced TNF-α release compared to cells exposed to the respective wild-type proteins. Importantly, the conservation of these residues across PYHIN proteins in both humans and mice underscores their evolutionary significance and offers insights into their potential role in species-wide inflammatory responses. The crucial role of these conserved residues is further substantiated by SPR analysis, revealing impaired binding of the IFI16-PYD mutants to the TLR4/MD2 complex compared to that of the IFI16^{FL} isoform. Conversely, mutating the widely conserved non-polar amino acid Ile17 in IFI16-PYD does not affect the IFI16^{FL}/TLR4 binding kinetic.

Overall, our findings unveil a central role of the PYHIN^{PYD} in mediating the binding to the TLR4/MD2 complex, subsequently triggering the transcriptional activation and release of pro-inflammatory cytokines in the extracellular milieu.[32,64] Further research is required to rule out that none of the other PYD-containing proteins outside the PYHIN families may share similar activities.

While our research does not directly link extracellular IFI16 to any specific human disease, there is substantial evidence of enhanced levels of circulating IFI16 protein or specific antibodies in multiple autoimmune/autoinflammatory conditions.[30,65,66] Remarkably, we show that IFI16 can induce inflammatory cell recruitment when intraperitoneally injected in mice as well as a pro-fibrotic skin phenotype upon intradermal injection. Consistently, our reanalysis of human SSc transcriptomes revealed a significant correlation between IFI16 mRNA expression levels and the overall inflammatory profile of the skin SSc biopsies. Moreover, other interferon-inducible proteins implicated in the inhibition of viral replication have also been recognized for their ability to be secreted and participate in cell-to-cell signaling.[67] Thus, our research adds to the body of evidence that IFI16, possibly together with other PYHIN family members, once abnormally released into the microenvironment, actively contributes to the uncontrolled immune responses observed in both sterile and infection-related inflammation due to its DAMP activity. Consequently, we propose a novel mechanism for sustaining chronic inflammation through IFI16-mediated intercellular communication, which warrants careful design and selection of PYHIN^{PYDs} inhibitors as potential treatments for autoimmune and autoinflammatory diseases.

Limitations of the study

The primary limitation of our study is the lack of experiments using a TLR4KO animal model to confirm that PYHIN PYD-induced inflammation occurs through the TLR4 signaling pathway *in vivo*. Additionally, questions remain about the translatability of our findings to clinical settings. While substantial evidence indicates elevated levels of circulating IFI16 protein or specific antibodies in multiple autoimmune and autoinflammatory conditions, further research is needed to determine whether IFI16 targeting is a viable therapeutic strategy *in vivo*. Finally, even if no other PYD-containing proteins outside the PYHIN family exhibit the same activities as IFI16, a definitive experiment would involve introducing the three K residues into NLRP3 or ASC PYD to assess whether they, like IFI16 and IFI16PYD, activate TLR4.

RESOURCE AVAILABILITY

Lead contact

Further information and requests for resources and reagents should be directed to and will be fulfilled by the lead contact, Marco De Andrea (marco.deandrea@unito.it).

Materials availability

This study did not generate new unique reagents, and all materials in this study are commercially available. The plasmids used in this study and any

additional analysis information for this work is available by request to the lead contact.

Data and code availability

- All the datasets used in this study were retrieved from public repositories. Gene Expression Omnibus (GEO) accession numbers are listed in the key resources table.
- This paper does not include the original code.
- Any additional information required to reanalyze the data reported in this paper is available from the lead contact upon request.

ACKNOWLEDGMENTS

We thank Stefano Garagnani and Veronica Martini (CAAD Center, Novara 28100, Italy) for help with skin histology and flow cytometry analysis, respectively, and the Flow Cytometry and Microscopy Core Facilities at the CAAD Center, Novara 28100, Italy. We thank Marcello Arsura for critically reviewing the manuscript.

This work was supported by the University of Turin (RILO2022 and RILO2023 to M.D.A.), by the Ministry of Education, University and Research – MUR (PRIN Projects 2022 P20222YKP8 to M.G.), and by EU funding within the MUR PNRR Extended Partnership initiative on Emerging Infectious Diseases (Project no. PE00000007, INF-ACT to M.D.A). A.I. is a Fulbright Research Scholar Award recipient. F.C. is the recipient of a PhD fellowship co-funded by Bristol Myers Squibb Italy under the MUR PNRR initiative (ex DM 630/2024).

The Graphical abstract was created in BioRender (De Andrea, M. (2025) https://BioRender.com/d19u452).

AUTHOR CONTRIBUTIONS

Conceptualization, A.I., I.Z., M.G., and M.D.A.; methodology, A.I., D.L., V.C., S. R., A.B., C.P., R.M., and M.D.A.; investigation, A.I., D.L., V.C., S.R., F.C., C.P., and R.M.; formal analysis, A.I., D.L., C.P., R.M., and M.D.A.; writing – original draft, A.I., M.G., and M.D.A.; writing – review and editing, A.I., D.L., C.P., I.Z., M.G., and M.D.A.; funding acquisition, A.I., M.G., and M.D.A.; resources, C.P., R.M., I.Z., M.G., and M.D.A.; and all authors read and approved the final manuscript.

DECLARATION OF INTERESTS

The authors declare no competing interests.

STAR★METHODS

Detailed methods are provided in the online version of this paper and include the following:

- KEY RESOURCES TABLE
- EXPERIMENTAL MODEL AND STUDY PARTICIPANT DETAILS
  - Cell lines and isolation of human PBMCs
  - Mice experiments
- METHOD DETAILS
  - Reagents, antibodies, and recombinant proteins
  - Cell treatments
  - Sequence alignments, protein structure prediction, docking, and mutagenesis
  - Co-immunoprecipitation and immunoblotting
  - Gene expression analysis
  - Cytokine measurement by ELISA
  - Surface plasmon resonance
  - Flow cytometry
  - Skin histology
  - PI permeabilization assay
  - Bioinformatics analysis
- QUANTIFICATION AND STATISTICAL ANALYSIS

SUPPLEMENTAL INFORMATION

Supplemental information can be found online at https://doi.org/10.1016/j.isci.2025.112413.

Received: September 9, 2024
Revised: March 2, 2025
Accepted: April 8, 2025
Published: April 11, 2025

REFERENCES

1. Mondini, M., Costa, S., Sponza, S., Gugliesi, F., Gariglio, M., and Landolfo, S. (2010). The interferon-inducible HIN-200 gene family in apoptosis and inflammation: implication for autoimmunity. Autoimmunity *43*, 226–231. https://doi.org/10.3109/08916930903510922.
2. Dawson, M.J., and Trapani, J.A. (1996). HIN-200: a novel family of IFN-inducible nuclear proteins expressed in leukocytes. J. Leukoc. Biol. *60*, 310–316.
3. Yan, H., Dalal, K., Hon, B.K., Youkharibache, P., Lau, D., and Pio, F. (2008). RPA nucleic acid-binding properties of IFI16-HIN200. Biochim. Biophys. Acta *1784*, 1087–1097. https://doi.org/10.1016/j.bbapap.2008.04.004.
4. Krieg, A.M. (2009). AIMing 2 detect foreign DNA. Sci. Signal. *2*, pe39. https://doi.org/10.1126/scisignal.277pe39.
5. Hornung, V., Ablasser, A., Charrel-Dennis, M., Bauernfeind, F., Horvath, G., Caffrey, D.R., Latz, E., and Fitzgerald, K.A. (2009). AIM2 recognizes cytosolic dsDNA and forms a caspase-1-activating inflammasome with ASC. Nature *458*, 514–518. https://doi.org/10.1038/nature07725.
6. Unterholzner, L., Keating, S.E., Baran, M., Horan, K.A., Jensen, S.B., Sharma, S., Sirois, C.M., Jin, T., Latz, E., Xiao, T.S., et al. (2010). IFI16 is an innate immune sensor for intracellular DNA. Nat. Immunol. *11*, 997–1004. https://doi.org/10.1038/ni.1932.
7. Brunette, R.L., Young, J.M., Whitley, D.G., Brodsky, I.E., Malik, H.S., and Stetson, D.B. (2012). Extensive evolutionary and functional diversity among mammalian AIM2-like receptors. J. Exp. Med. *209*, 1969–1983. https://doi.org/10.1084/jem.20121960.
8. Loeven, N.A., Medici, N.P., and Bliska, J.B. (2020). The pyrin inflammasome in host–microbe interactions. Curr. Opin. Microbiol. *54*, 77–86. https://doi.org/10.1016/j.mib.2020.01.005.
9. Falcone, E.L., and Bryant, C. (2019). Let's get this pyrin started. J. Biol. Chem. *294*, 3367–3368. https://doi.org/10.1074/jbc.H119.007830.
10. Justice, J.L., and Cristea, I.M. (2022). Nuclear antiviral innate responses at the intersection of DNA sensing and DNA repair. Trends Microbiol. *30*, 1056–1071. https://doi.org/10.1016/j.tim.2022.05.004.
11. Almine, J.F., O'Hare, C.A.J., Dunphy, G., Haga, I.R., Naik, R.J., Atrih, A., Connolly, D.J., Taylor, J., Kelsall, I.R., Bowie, A.G., et al. (2017). IFI16 and cGAS cooperate in the activation of STING during DNA sensing in human keratinocytes. Nat. Commun. *8*, 14392. https://doi.org/10.1038/ncomms14392.
12. Jakobsen, M.R., and Paludan, S.R. (2014). IFI16: At the interphase between innate DNA sensing and genome regulation. Cytokine Growth Factor Rev. *25*, 649–655. https://doi.org/10.1016/j.cytogfr.2014.06.004.
13. Ouchi, M., and Ouchi, T. (2008). Role of IFI16 in DNA damage and checkpoint. Front. Biosci. *13*, 236–239.
14. Gariano, G.R., Dell'Oste, V., Bronzini, M., Gatti, D., Luganini, A., De Andrea, M., Gribaudo, G., Gariglio, M., and Landolfo, S. (2012). The intracellular DNA sensor IFI16 gene acts as restriction factor for human cytomegalovirus replication. PLoS Pathog. *8*, e1002498. https://doi.org/10.1371/journal.ppat.1002498.
15. Lo Cigno, I., De Andrea, M., Borgogna, C., Albertini, S., Landini, M.M., Peretti, A., Johnson, K.E., Chandran, B., Landolfo, S., and Gariglio, M. (2015). The Nuclear DNA Sensor IFI16 Acts as a Restriction Factor for Human Papillomavirus Replication through Epigenetic Modifications of the Viral Promoters. J. Virol. *89*, 7506–7520. https://doi.org/10.1128/JVI.00013-15.

16. Mishra, S., Raj, A.S., Kumar, A., Rajeevan, A., Kumari, P., and Kumar, H. (2022). Innate immune sensing of influenza A viral RNA through IFI16 promotes pyroptotic cell death. iScience *25*, 103714. https://doi.org/10.1016/j.isci.2021.103714.

17. Caneparo, V., Pastorelli, L., Pisani, L.F., Bruni, B., Prodam, F., Boldorini, R., Roggenbuck, D., Vecchi, M., Landolfo, S., Gariglio, M., and De Andrea, M. (2016). Distinct Anti-IFI16 and Anti-GP2 Antibodies in Inflammatory Bowel Disease and Their Variation with Infliximab Therapy. Inflamm. Bowel Dis. *22*, 2977–2987. https://doi.org/10.1097/MIB.0000000000000926.

18. Vanhove, W., Peeters, P.M., Staelens, D., Schraenen, A., Van der Goten, J., Cleynen, I., De Schepper, S., Van Lommel, L., Reynaert, N.L., Schuit, F., et al. (2015). Strong Upregulation of AIM2 and IFI16 Inflammasomes in the Mucosa of Patients with Active Inflammatory Bowel Disease. Inflamm. Bowel Dis. *21*, 2673–2682. https://doi.org/10.1097/MIB.0000000000000535.

19. Costa, S., Borgogna, C., Mondini, M., De Andrea, M., Meroni, P.L., Berti, E., Gariglio, M., and Landolfo, S. (2011). Redistribution of the nuclear protein IFI16 into the cytoplasm of ultraviolet B-exposed keratinocytes as a mechanism of autoantigen processing. Br. J. Dermatol. *164*, 282–290. https://doi.org/10.1111/j.1365-2133.2010.10097.x.

20. Mondini, M., Vidali, M., Airò, P., De Andrea, M., Riboldi, P., Meroni, P.L., Gariglio, M., and Landolfo, S. (2007). Role of the interferon-inducible gene IFI16 in the etiopathogenesis of systemic autoimmune disorders. Ann. N. Y. Acad. Sci. *1110*, 47–56. https://doi.org/10.1196/annals.1423.006.

21. Alunno, A., Caneparo, V., Carubbi, F., Bistoni, O., Caterbi, S., Bartoloni, E., Giacomelli, R., Gariglio, M., Landolfo, S., and Gerli, R. (2015). Interferon gamma-inducible protein 16 in primary Sjögren's syndrome: a novel player in disease pathogenesis? Arthritis Res. Ther. *17*, 208. https://doi.org/10.1186/s13075-015-0722-2.

22. Alunno, A., Bartoloni, E., Bistoni, O., Gerli, R., Caneparo, V., Carubbi, F., and Landolfo, S. (2017). Relevance of Interferon-Inducible Protein-16 Rather than Anti-Interferon-Inducible Protein-16 Autoantibodies as a Clinical and Pathogenic Biomarker in Primary Sjögren's Syndrome: Comment on the Article by Baer et al. Arthritis Care Res. *69*, 453–454. https://doi.org/10.1002/acr.22918.

23. Cao, T., Shao, S., Li, B., Jin, L., Lei, J., Qiao, H., and Wang, G. (2016). Up-regulation of Interferon-inducible protein 16 contributes to psoriasis by modulating chemokine production in keratinocytes. Sci. Rep. *6*, 25381. https://doi.org/10.1038/srep25381.

24. Chiliveru, S., Rahbek, S.H., Jensen, S.K., Jørgensen, S.E., Nissen, S.K., Christiansen, S.H., Mogensen, T.H., Jakobsen, M.R., Iversen, L., Johansen, C., and Paludan, S.R. (2014). Inflammatory cytokines break down intrinsic immunological tolerance of human primary keratinocytes to cytosolic DNA. J. Immunol. *192*, 2395–2404. https://doi.org/10.4049/jimmunol.1302120.

25. Tervaniemi, M.H., Katayama, S., Skoog, T., Siitonen, H.A., Vuola, J., Nuutila, K., Sormunen, R., Johnsson, A., Linnarsson, S., Suomela, S., et al. (2016). NOD-like receptor signaling and inflammasome-related pathways are highlighted in psoriatic epidermis. Sci. Rep. *6*, 22745. https://doi.org/10.1038/srep22745.

26. Mondini, M., Vidali, M., De Andrea, M., Azzimonti, B., Airò, P., D'Ambrosio, R., Riboldi, P., Meroni, P.L., Albano, E., Shoenfeld, Y., et al. (2006). A novel autoantigen to differentiate limited cutaneous systemic sclerosis from diffuse cutaneous systemic sclerosis: the interferon-inducible gene IFI16. Arthritis Rheum. *54*, 3939–3944. https://doi.org/10.1002/art.22266.

27. Alunno, A., Caneparo, V., Bistoni, O., Caterbi, S., Terenzi, R., Gariglio, M., Bartoloni, E., Manzo, A., Landolfo, S., and Gerli, R. (2016). Circulating Interferon-Inducible Protein IFI16 Correlates With Clinical and Serological Features in Rheumatoid Arthritis. Arthritis Care Res. *68*, 440–445. https://doi.org/10.1002/acr.22695.

28. Baer, A.N., Petri, M., Sohn, J., Rosen, A., and Casciola-Rosen, L. (2016). Association of Antibodies to Interferon-Inducible Protein-16 With Markers of More Severe Disease in Primary Sjögren's Syndrome. Arthritis Care Res. *68*, 254–260. https://doi.org/10.1002/acr.22632.

29. Caneparo, V., Cena, T., De Andrea, M., Dell'oste, V., Stratta, P., Quaglia, M., Tincani, A., Andreoli, L., Ceffa, S., Taraborelli, M., et al. (2013). Anti-IFI16 antibodies and their relation to disease characteristics in systemic lupus erythematosus. Lupus *22*, 607–613. https://doi.org/10.1177/0961203313484978.

30. De Andrea, M., De Santis, M., Caneparo, V., Generali, E., Sirotti, S., Isailovic, N., Guidelli, G.M., Ceribelli, A., Fabbroni, M., Simpatico, A., et al. (2020). Serum IFI16 and anti-IFI16 antibodies in psoriatic arthritis. Clin. Exp. Immunol. *199*, 88–96. https://doi.org/10.1111/cei.13376.

31. Uchida, K., Akita, Y., Matsuo, K., Fujiwara, S., Nakagawa, A., Kazaoka, Y., Hachiya, H., Naganawa, Y., Oh-Iwa, I., Ohura, K., et al. (2005). Identification of specific autoantigens in Sjögren's syndrome by SEREX. Immunology *116*, 53–63. https://doi.org/10.1111/j.1365-2567.2005.02197.x.

32. Iannucci, A., Caneparo, V., Raviola, S., Debernardi, I., Colangelo, D., Miggiano, R., Griffante, G., Landolfo, S., Gariglio, M., and De Andrea, M. (2020). Toll-like receptor 4-mediated inflammation triggered by extracellular IFI16 is enhanced by lipopolysaccharide binding. PLoS Pathog. *16*, e1008811. https://doi.org/10.1371/journal.ppat.1008811.

33. Kim, D.E., Chivian, D., and Baker, D. (2004). Protein structure prediction and analysis using the Robetta server. Nucleic Acids Res. *32*, W526–W531. https://doi.org/10.1093/nar/gkh468.

34. van Zundert, G.C.P., Rodrigues, J.P.G.L.M., Trellet, M., Schmitz, C., Kastritis, P.L., Karaca, E., Melquiond, A.S.J., van Dijk, M., de Vries, S.J., and Bonvin, A.M.J.J. (2016). The HADDOCK2.2 Web Server: User-Friendly Integrative Modeling of Biomolecular Complexes. J. Mol. Biol. *428*, 720–725. https://doi.org/10.1016/j.jmb.2015.09.014.

35. Bhattacharyya, S., Wang, W., Qin, W., Cheng, K., Coulup, S., Chavez, S., Jiang, S., Raparia, K., De Almeida, L.M.V., Stehlik, C., et al. (2018). TLR4-dependent fibroblast activation drives persistent organ fibrosis in skin and lung. JCI Insight *3*, e98850. https://doi.org/10.1172/jci.insight.98850.

36. Li, F.J., Surolia, R., Li, H., Wang, Z., Liu, G., Kulkarni, T., Massicano, A.V.F., Mobley, J.A., Mondal, S., de Andrade, J.A., et al. (2021). Citrullinated vimentin mediates development and progression of lung fibrosis. Sci. Transl. Med. *13*, eaba2927. https://doi.org/10.1126/scitranslmed.aba2927.

37. Błyszczuk, P., Kozlova, A., Guo, Z., Kania, G., and Distler, O. (2019). Experimental Mouse Model of Bleomycin-Induced Skin Fibrosis. Curr. Protoc. Immunol. *126*, e88. https://doi.org/10.1002/cpim.88.

38. Milano, A., Pendergrass, S.A., Sargent, J.L., George, L.K., McCalmont, T. H., Connolly, M.K., and Whitfield, M.L. (2008). Molecular Subsets in the Gene Expression Signatures of Scleroderma Skin. PLoS One *3*, e2696. https://doi.org/10.1371/journal.pone.0002696.

39. Marongiu, L., Gornati, L., Artuso, I., Zanoni, I., and Granucci, F. (2019). Below the surface: The inner lives of TLR4 and TLR9. J. Leukoc. Biol. *106*, 147–160. https://doi.org/10.1002/JLB.3MIR1218-483RR.

40. Ii, M., Matsunaga, N., Hazeki, K., Nakamura, K., Takashima, K., Seya, T., Hazeki, O., Kitazaki, T., and Iizawa, Y. (2006). A Novel Cyclohexene Derivative, Ethyl (6R)-6-[N-(2-Chloro-4-fluorophenyl)sulfamoyl]cyclohex-1-ene-1-carboxylate (TAK-242), Selectively Inhibits Toll-Like Receptor 4-Mediated Cytokine Production through Suppression of Intracellular Signaling. Mol. Pharmacol. *69*, 1288–1295. https://doi.org/10.1124/mol.105.019695.

41. Hajjar, A.M., Ernst, R.K., Tsai, J.H., Wilson, C.B., and Miller, S.I. (2002). Human Toll-like receptor 4 recognizes host-specific LPS modifications. Nat. Immunol. *3*, 354–359. https://doi.org/10.1038/ni777.

42. Cridland, J.A., Curley, E.Z., Wykes, M.N., Schroder, K., Sweet, M.J., Roberts, T.L., Ragan, M.A., Kassahn, K.S., and Stacey, K.J. (2012). The mammalian PYHIN gene family: phylogeny, evolution and expression. BMC Evol. Biol. *12*, 140. https://doi.org/10.1186/1471-2148-12-140.

43. French FMF Consortium (1997). A candidate gene for familial Mediterranean fever. Nat. Genet. *17*, 25–31. https://doi.org/10.1038/ng0997-25.

44. Weber, F. (2015). The catcher in the RIG-I. Cytokine *76*, 38–41. https://doi.org/10.1016/j.cyto.2015.07.002.

45. Fairbrother, W.J., Gordon, N.C., Humke, E.W., O'Rourke, K.M., Starovasnik, M.A., Yin, J.-P., and Dixit, V.M. (2001). The PYRIN domain: A member of the death domain-fold superfamily. Protein Sci. *10*, 1911–1918. https://doi.org/10.1110/ps.13801.

46. Liepinsh, E., Barbals, R., Dahl, E., Sharipo, A., Staub, E., and Otting, G. (2003). The death-domain fold of the ASC PYRIN domain, presenting a basis for PYRIN/PYRIN recognition. J. Mol. Biol. *332*, 1155–1163. https://doi.org/10.1016/j.jmb.2003.07.007.

47. Chu, L.H., Gangopadhyay, A., Dorfleutner, A., and Stehlik, C. (2015). An updated view on the structure and function of PYRIN domains. Apoptosis *20*, 157–173. https://doi.org/10.1007/s10495-014-1065-1.

48. de Alba, E. (2019). Structure, interactions and self-assembly of ASC-dependent inflammasomes. Arch. Biochem. Biophys. *670*, 15–31. https://doi.org/10.1016/j.abb.2019.05.023.

49. Jin, T., Perry, A., Jiang, J., Smith, P., Curry, J.A., Unterholzner, L., Jiang, Z., Horvath, G., Rathinam, V.A., Johnstone, R.W., et al. (2012). Structures of the HIN domain:DNA complexes reveal ligand binding and activation mechanisms of the AIM2 inflammasome and IFI16 receptor. Immunity *36*, 561–571. https://doi.org/10.1016/j.immuni.2012.02.014.

50. Zhou, R., Yazdi, A.S., Menu, P., and Tschopp, J. (2011). A role for mitochondria in NLRP3 inflammasome activation. Nature *469*, 221–225. https://doi.org/10.1038/nature09663.

51. Broz, P., and Dixit, V.M. (2016). Inflammasomes: mechanism of assembly, regulation and signalling. Nat. Rev. Immunol. *16*, 407–420. https://doi.org/10.1038/nri.2016.58.

52. Ma, M., Jiang, W., and Zhou, R. (2024). DAMPs and DAMP-sensing receptors in inflammation and diseases. Immunity *57*, 752–771. https://doi.org/10.1016/j.immuni.2024.03.002.

53. Lamkanfi, M., Vande Walle, L., and Kanneganti, T.-D. (2011). Deregulated inflammasome signaling in disease. Immunol. Rev. *243*, 163–173. https://doi.org/10.1111/j.1600-065X.2011.01042.x.

54. The International FMF Consortium (1997). Ancient Missense Mutations in a New Member of the RoRet Gene Family Are Likely to Cause Familial Mediterranean Fever. Cell *90*, 797–807. https://doi.org/10.1016/S0092-8674(00)80539-5.

55. Ozen, S. (2021). Update in familial Mediterranean fever. Curr. Opin. Rheumatol. *33*, 398–402. https://doi.org/10.1097/BOR.0000000000000821.

56. Park, Y.H., Wood, G., Kastner, D.L., and Chae, J.J. (2016). Pyrin inflammasome activation and RhoA signaling in the autoinflammatory diseases FMF and HIDS. Nat. Immunol. *17*, 914–921. https://doi.org/10.1038/ni.3457.

57. Ben-Chetrit, E., Gattorno, M., Gul, A., Kastner, D.L., Lachmann, H.J., Touitou, I., and Ruperto, N.; Paediatric Rheumatology International Trials Organisation PRINTO and the AIDs Delphi study participants (2018). Consensus proposal for taxonomy and definition of the autoinflammatory diseases (AIDs): a Delphi study. Ann. Rheum. Dis. *77*, 1558–1565. https://doi.org/10.1136/annrheumdis-2017-212515.

58. Hoffman, H.M., Kuemmerle-Deschner, J.B., and Goldbach-Mansky, R. (2019). Cryopyrin-Associated Periodic Syndromes (CAPS). In Textbook of Autoinflammation, P.J. Hashkes, R.M. Laxer, and A. Simon, eds. (Springer International Publishing), pp. 347–365. https://doi.org/10.1007/978-3-319-98605-0_19.

59. Agostini, L., Martinon, F., Burns, K., McDermott, M.F., Hawkins, P.N., and Tschopp, J. (2004). NALP3 Forms an IL-1β-Processing Inflammasome with Increased Activity in Muckle-Wells Autoinflammatory Disorder. Immunity *20*, 319–325. https://doi.org/10.1016/S1074-7613(04)00046-9.

60. de Souza, J.G., Starobinas, N., and Ibañez, O.C.M. (2021). Unknown/enigmatic functions of extracellular ASC. Immunology *163*, 377–388. https://doi.org/10.1111/imm.13375.

61. Franklin, B.S., Bossaller, L., De Nardo, D., Ratter, J.M., Stutz, A., Engels, G., Brenker, C., Nordhoff, M., Mirandola, S.R., Al-Amoudi, A., et al. (2014). The adaptor ASC has extracellular and "prionoid" activities that propagate inflammation. Nat. Immunol. *15*, 727–737. https://doi.org/10.1038/ni.2913.

62. Baroja-Mazo, A., Martín-Sánchez, F., Gomez, A.I., Martínez, C.M., Amores-Iniesta, J., Compan, V., Barberà-Cremades, M., Yagüe, J., Ruiz-Ortiz, E., Antón, J., et al. (2014). The NLRP3 inflammasome is released as a particulate danger signal that amplifies the inflammatory response. Nat. Immunol. *15*, 738–748. https://doi.org/10.1038/ni.2919.

63. Gaul, S., Schaeffer, K.M., Opitz, L., Maeder, C., Kogel, A., Uhlmann, L., Kalwa, H., Wagner, U., Haas, J., Behzadi, A., et al. (2021). Extracellular NLRP3 inflammasome particles are internalized by human coronary artery smooth muscle cells and induce pro-atherogenic effects. Sci. Rep. *11*, 15156. https://doi.org/10.1038/s41598-021-94314-1.

64. Gong, T., Liu, L., Jiang, W., and Zhou, R. (2020). DAMP-sensing receptors in sterile inflammation and inflammatory diseases. Nat. Rev. Immunol. *20*, 95–112. https://doi.org/10.1038/s41577-019-0215-7.

65. Antiochos, B., Trejo-Zambrano, D., Fenaroli, P., Rosenberg, A., Baer, A., Garg, A., Sohn, J., Li, J., Petri, M., Goldman, D.W., et al. (2022). The DNA sensors AIM2 and IFI16 are SLE autoantigens that bind neutrophil extracellular traps. Elife *11*, e72103. https://doi.org/10.7554/eLife.72103.

66. Caneparo, V., Landolfo, S., Gariglio, M., and De Andrea, M. (2018). The Absent in Melanoma 2-Like Receptor IFN-Inducible Protein 16 as an Inflammasome Regulator in Systemic Lupus Erythematosus: The Dark Side of Sensing Microbes. Front. Immunol. *9*, 1180. https://doi.org/10.3389/fimmu.2018.01180.

67. Swaim, C.D., Scott, A.F., Canadeo, L.A., and Huibregtse, J.M. (2017). Extracellular ISG15 Signals Cytokine Secretion through the LFA-1 Integrin Receptor. Mol. Cell *68*, 581–590.e5. https://doi.org/10.1016/j.molcel.2017.10.003.

68. Gariglio, M., Azzimonti, B., Pagano, M., Palestro, G., De Andrea, M., Valente, G., Voglino, G., Navino, L., and Landolfo, S. (2002). Immunohistochemical expression analysis of the human interferon-inducible gene IFI16, a member of the HIN200 family, not restricted to hematopoietic cells. J. Interferon Cytokine Res. *22*, 815–821. https://doi.org/10.1089/107999002320271413.

69. Pendergrass, S.A., Lemaire, R., Francis, I.P., Mahoney, J.M., Lafyatis, R., and Whitfield, M.L. (2012). Intrinsic gene expression subsets of diffuse cutaneous systemic sclerosis are stable in serial skin biopsies. J. Invest. Dermatol., 1363–1373. https://doi.org/10.1038/jid.2011.472.

70. Hinchcliff, M., Huang, C.C., Wood, T.A., Matthew Mahoney, J., Martyanov, V., Bhattacharyya, S., Tamaki, Z., Lee, J., Carns, M., Podlusky, S., et al. (2013). Molecular signatures in skin associated with clinical improvement during mycophenolate treatment in systemic sclerosis. J. Invest. Dermatol., 1979–1989. https://doi.org/10.1038/jid.2013.130.

71. Kumar, S., Stecher, G., Li, M., Knyaz, C., Tamura, K., and MEGA, X. (2018). Molecular Evolutionary Genetics Analysis across Computing Platforms. Mol. Biol. Evol., 1547–1549. https://doi.org/10.1093/molbev/msy096.

72. Thompson, J.D., Higgins, D.G., and Gibson, T.J. (1994). CLUSTAL W: improving the sensitivity of progressive multiple sequence alignment through sequence weighting, position-specific gap penalties and weight matrix choice. Nucleic Acids Res. *22*, 4673–4680. https://doi.org/10.1093/nar/22.22.4673.

73. Barrett, T., Wilhite, S.E., Ledoux, P., Evangelista, C., Kim, I.F., Tomashevsky, M., Marshall, K.A., Phillippy, K.H., Sherman, P.M., Holko, M., et al. (2013). NCBI GEO: archive for functional genomics data sets–update. Nucleic Acids Res. *41*, D991–D995. https://doi.org/10.1093/nar/gks1193.

74. Porta, C., Rimoldi, M., Raes, G., Brys, L., Ghezzi, P., Di Liberto, D., Dieli, F., Ghisletti, S., Natoli, G., De Baetselier, P., et al. (2009). Tolerance and M2 (alternative) macrophage polarization are related processes orchestrated by p50 nuclear factor kappaB. Proc. Natl. Acad. Sci. USA *106*, 14978–14983. https://doi.org/10.1073/pnas.0809784106.

75. Raviola, S., Griffante, G., Iannucci, A., Chandel, S., Lo Cigno, I., Lacarbonara, D., Caneparo, V., Pasquero, S., Favero, F., Corà, D., et al. (2024). Human cytomegalovirus infection triggers a paracrine senescence loop in renal epithelial cells. Commun. Biol. *7*, 292. https://doi.org/10.1038/s42003-024-05957-5.

STAR★METHODS

KEY RESOURCES TABLE

REAGENT or RESOURCE	SOURCE	IDENTIFIER
Antibodies		
Rabbit polyclonal anti-IFI16 N-term	Gariglio et al.,[68]	N/A
Rabbit polyclonal anti-IFI16 C-term	Gariglio et al.,[68]	N/A
Mouse anti-human TLR4 monoclonal antibody	Santa Cruz Biotechnology	Cat# sc-293072: RRID:AB_10611320
Mouse anti-human TLR4 monoclonal antibody	Santa Cruz Biotechnology	Cat# sc-13593; RRID: AB_628366
Mouse anti-β-actin monoclonal antibody	Sigma-Aldrich	Cat# A1978; RRID: AB_476692
Goat anti-rabbit IgG-HRP	Sigma-Aldrich	Cat# A6154; RRID: AB_258284
Goat anti-mouse IgG-HRP	Thermo Fisher Scientifc	Cat# A16072; RRID: AB_ 2534745
Alexa Fluor 488 anti-mouse/human CD11b antibody	BioLegend	Cat# 101219; RRID: AB_493545
APC/Cyanine7 anti-mouse Ly-6C Antibody	BioLegend	Cat# 128025; RRID: AB_10643867
Brilliant Violet 711 anti-mouse Ly-6G Antibody	BioLegend	Cat# 127643; RRID: AB_2565971
APC anti-mouse F4/80 Antibody	BioLegend	Cat# 123115; RRID: AB_893493
PE anti-mouse I-A/I-E Antibody	BioLegend	Cat# 107607; RRID: AB_313322
Brilliant Violet 650 anti-mouse CD86 Antibody	BioLegend	Cat# 105035; RRID: AB_11126147
Bacterial and virus strains		
ClearColi BL21(DE3)	Lucigen	Cat# 60810
Chemicals, peptides, and recombinant proteins		
CLI-095	Invivogen	Cat# tlrl-cli95-4
Phorbol 12-myristate 13-acetate	Sigma-Aldrich	Cat# P8139
Human recombinant IFI16^{FL}	Iannucci et al.,[32]	N/A
Human recombinant IFI16 PYD	Iannucci et al.,[32]	N/A
Human recombinant IFI16 HINA	Iannucci et al.,[32]	N/A
Human recombinant IFI16 HINB	Iannucci et al.,[32]	N/A
Human recombinant IFI16ΔHINB	Iannucci et al.,[32]	N/A
Human recombinant IFI16ΔPYD	This paper	N/A
Human recombinant IFI16^{FL}-I17A	This paper	N/A
Human recombinant IFI16^{FL}-K34A	This paper	N/A
Human recombinant IFI16^{FL}-K64G	This paper	N/A
Human recombinant IFI16^{FL}-K86A	This paper	N/A
Human recombinant IFI16^{FL}-K34A/K64G/K86A	This paper	N/A
Human recombinant IFI16^{PYD}-K34A/K64G/K86A	This paper	N/A
Human recombinant ASC PYD	This paper	N/A
Human recombinant NLRP3 PYD	This paper	N/A
Human recombinant IFIX PYD	This paper	N/A
Human recombinant MNDA PYD	This paper	N/A
Human recombinant AIM2 PYD	This paper	N/A
Mouse recombinant aim2 PYD	This paper	N/A
Mouse recombinant ifi203 PYD	This paper	N/A
Mouse recombinant ifi204 PYD	This paper	N/A
Human recombinant TLR4/MD2 complex protein	R&D systems	Cat# 3146-TM-050/CF
RPMI medium 1640	Sigma-Aldrich	Cat# R0883
Hank's Buffered Saline Solution	Lonza	Cat# 10-508Q
Bovine serum albumin (BSA)	Sigma-Aldrich	Cat# A7030
Fetal Bovine Serum (FBS)	Immunological Sciences	Cat# EU-000-500

(*Continued on next page*)

Continued

REAGENT or RESOURCE	SOURCE	IDENTIFIER
Penicillin/Streptomycin/Gentamycin solution	Gibco	Cat# 10378-016
Propidium Iodide	Sigma-Aldrich	Cat# 537059
Histopaque	Sigma-Aldrich	Cat# 1077-1
Percoll	Cytiva	Cat# GEH17089101
Protease inhibitor cocktail	Thermo Fisher Scientifc	Cat# 1860932
Phosphatase inhibitor cocktail	Thermo Fisher Scientifc	Cat# 78420
TRIzol Reagent	Thermo Fisher Scientifc	Cat# 15596026
SsoAdvanced Universal SYBR Green Supermix	Bio-Rad	Cat# 1725274
HBS-EP+ Buffer 10x	Cytiva	Cat# BR100669
Bleomycin sulfate	Santa Cruz Biotechnology	Cat# sc-200134
Critical commercial assays		
TGX™ FastCast™ Acrylamide Kit, 7.5%	Bio-Rad	Cat# 1610171
TGX™ FastCast™ Acrylamide Kit, 12%	Bio-Rad	Cat# 1610175
Dynabeads Protein G Immunoprecipitation Kit	Thermo Fisher Scientific	Cat# 10007D
iScript cDNA synthesis kit	Bio-Rad	Cat# 1708890
Human IL-6 DuoSet ELISA	R&D systems	Cat# DY206
Human IL-8 DuoSet ELISA	R&D systems	Cat# DY208
Human TNF-α DuoSet ELISA	R&D systems	Cat# DY210
Mouse TNF-α DuoSet ELISA	R&D systems	Cat# DY410
ELISA MAX™ Deluxe Set Human TNF-α	BioLegend	Cat# 430204
ELISA MAX™ Deluxe Set Human IL-6	BioLegend	Cat# 430504
ELISA MAX™ Deluxe Set Human IL-1β	BioLegend	Cat# 437004
LIVE/DEAD™ Fixable Aqua Dead Cell Stain Kit, for 405 nm excitation	Thermo Fisher Scientific	Cat# L34966
Deposited data		
Sequence of human IFI16	Uniprot	Q16666
Sequence of human MNDA	Uniprot	P41218
Sequence of human AIM2	Uniprot	O14862
Sequence of human IFIX	Uniprot	Q6K0P9
Sequence of mouse ifi203	Uniprot	O35368
Sequence of mouse ifi204	Uniprot	P0DOV2
Sequence of mouse aim2	Uniprot	Q91VJ1
Sequence of mouse ifi205	Uniprot	Q8CGE8
Sequence of mouse ifi206	Uniprot	G3UZV2
Sequence of mouse ifi207	Uniprot	E9Q3L4
Sequence of mouse ifi208	Uniprot	Q3V3Q4
Sequence of mouse ifi209	Uniprot	Q8BV49
Sequence of mouse ifi211	Uniprot	P0DOV1
Sequence of mouse ifi212	Uniprot	D0QMC3
Sequence of mouse ifi213	Uniprot	Q3UPZ5
Sequence of mouse ifi214	Uniprot	Q504N7
Sequence of human NLRP3	Uniprot	Q96P20
Sequence of human ASC	Uniprot	Q9ULZ3
Gene Expression Profiling of Scleroderma Skin	Milano et al.,[38]	GEO: GSE9285
Gene Expression Profiling of Scleroderma Skin	Pendergrass et al.[69]	GEO: GSE32413
Gene Expression Profiling of Scleroderma Skin	Hinchcliff et al.[70]	GEO: GSE45485
Experimental models: Cell lines		
THP-1	ATCC	Cat# TIB-202; RRID: CVCL_0006
RAW 264.7	ATCC	Cat# TIB-71; RRID :CVCL_0493

(*Continued on next page*)

Continued

REAGENT or RESOURCE	SOURCE	IDENTIFIER
Experimental models: Organisms/strains		
C57BL6/J mice	The Jackson Laboratory	Cat#000664; RRID: IMSR_JAX:000664
Oligonucleotides		
TNFA Forward primer 5'-GCCAG AGGGCTGATTAGAGA-3'	This work	N/A
TNFA Reverse primer 5'- TCAGCCT CTTCTCCTTCCTG-3'	This work	N/A
IL8 Forward primer 5'- ATGACTTC CAAGCTGGCCGTGGCT-3'	This work	N/A
IL8 Reverse primer 5'- TCTCAGCC CTCTTCAAAAACTTCTC-3'	This work	N/A
IL1B Forward primer 5'- TCCCCA GCCCTTTTGTTGA-3'	This work	N/A
IL1B Reverse primer 5'- TTAGAA CCAAATGTGGCCGTG-3'	This work	N/A
GAPDH Forward primer 5'- AACGT GTCAGTGGTGGACCTG-3'	This work	N/A
GAPDH Reverse primer 5'- AGTGGG TGTCGCTGTTGAAGT-3'	This work	N/A
Recombinant DNA		
pET30a IFI16^{FL}	Iannucci et al.,[32]	N/A
pET30a IFI16 PYD	Iannucci et al.,[32]	N/A
pET30a IFI16 HINA	Iannucci et al.,[32]	N/A
pET30a IFI16 HINB	Iannucci et al.,[32]	N/A
pET30a IFI16ΔHINB	Iannucci et al.,[32]	N/A
pET30a IFI16ΔPYD	Genscript	N/A
pET30a IFI16^{FL}-I17A	Genscript	N/A
pET30a IFI16^{FL}-K34A	Genscript	N/A
pET30a IFI16^{FL}-K64G	Genscript	N/A
pET30a IFI16^{FL}-K86A	Genscript	N/A
pET30a IFI16^{FL}-K34A/K64G/K86A	Genscript	N/A
pET30a IFI16^{PYD}-K34A/K64G/K86A	Genscript	N/A
pET30a ASC PYD	Genscript	N/A
pET30a NLRP3 PYD	Genscript	N/A
pET30a IFIX PYD	Genscript	N/A
pET30a MNDA PYD	Genscript	N/A
pET30a AIM2 PYD	Genscript	N/A
pET30a aim2 PYD	Genscript	N/A
pET30a ifi203 PYD	Genscript	N/A
pET30a ifi204 PYD	Genscript	N/A
Software and algorithms		
GraphPad Prism version 9.00 for Windows	GraphPad, Software, La Jolla, California, USA	www.graphpad.com; RRID: SCR_022798
BIAcore Evaluation Software	GE Healtcare	https://www.biacore.com/lifesciences/service/downloads/software_licenses/biaevaluation/; RRID: SCR_015936
MEGAX software	Kumar et al.[71]	https://doi.org/10.1093/molbev/msy096; RRID: SCR_023471
ClustalW algorithm	Thompson et al.[72]	https://doi.org/10.1093/nar/22.22.4673; RRID: SCR_017277

(*Continued on next page*)

Continued

REAGENT or RESOURCE	SOURCE	IDENTIFIER
Robetta software	Kim et al.,[33]	https://doi.org/10.1093/nar/gkh468; RRID: SCR_018805
HADDOCK web server	Van Zundert et al.,[34]	https://doi.org/10.1016/j.jmb.2015.09.014; RRID: SCR_019091
PyMOL software	The PyMOL Molecular Graphics System, Version 2.3.4 Schrödinger, LLC	https://www.pymol.org/; RRID: SCR_000305
Flow Jo software, version 10.9	FlowJo LLC	https://www.flowjo.com/; RRID: SCR_008520
Slideviewer software, version 2.7	3DHISTECH	https://www.3dhistech.com/research/digital-microscopes-viewers/Slideviewer/
GEO2R web tool	Barrett et al.[73]	https://doi.org/10.1093/nar/gks1193; RRID: SCR_016569
Other		
Instant*Blue* Coomassie	Expedon	Cat# ISB1L
Westar Antares	Cyanagen	Cat# XLS042,250
Sensor chip CM5	Cytiva	Cat# BR100012

EXPERIMENTAL MODEL AND STUDY PARTICIPANT DETAILS

Cell lines and isolation of human PBMCs

Human leukemia monocytes THP-1 and murine macrophages RAW 264.7 were obtained from ATCC and grown at 37°C 5% of CO_2 in RPMI 1640 Medium (Sigma-Aldrich) containing 10% of fetal bovine serum (FBS, Immunological Sciences) and 1% of penicillin/streptomycin/glutamine solution (PSG, Gibco). THP-1 were differentiated into macrophages (M0) with 100 ng/ml PMA for 48 h followed by 24 h of resting period before treatment. Routine testing of cell lines for contamination with Mycoplasma was performed using a standard PCR method. Human peripheral blood mononuclear cells (PBMCs) or monocytes were isolated from the buffy coats of healthy donors' blood, obtained from the blood bank of Boston Children's Hospital. The samples were anonymous, and sex and gender are unknown. The sample size is indicated in the figure legend (see Figure S1). Briefly, blood was diluted 1:2 in PBS, and PBMCs were isolated using Histopaque (Sigma-Aldrich) gradient, and then resuspended in RPMI 1640 Medium supplemented with 10% FBS and 1% PSG. Monocytes were isolated by a well-established protocol based on two step density gradient centrifugation performed with Histopaque (Sigma-Aldrich) and 46% Percoll (Cytiva).[74] Finally, to eliminate remaining lymphocytes, cells were seeded in RPMI 1640 Medium supplemented 1% PSG and incubated at 37°C 5% CO_2 to allow monocyte attachment. After 1h of incubation, non-adherent cells were vigorously washed out with saline solution and monocytes were cultured in RPMI 1640 Medium supplemented with 10% FBS and 1% PSG.

Mice experiments

C57BL/6J mice were acquired from The Jackson Laboratory. Mice were housed under specific pathogen-free condition, and all the procedures were approved by the Institutional Animal Care and Use Committee (IACUC) of Boston Children's Hospital (ethical approval number 1995). Eight-week-old female mice were used for the *in vivo* experiments. For inflammatory cell recruitment, mice were intraperitoneally (i.p.) injected with recombinant $IFI16^{FL}$ (5 mg/kg), $IFI16^{PYD}$ (5 mg/kg), IFI16ΔPYD (5 mg/kg) or with vehicle as control. Twenty-four hours after the treatment, mice were euthanized by CO_2 inhalation. Peritoneal exudate cells (PECs) were recovered by peritoneal lavage using 5 ml of PBS and analyzed using flow cytometry.

For the experimental model of fibrosis, mice received subcutaneous (s.c.) injections of bleomycin (0.1 units/mice), recombinant IFI16 ($IFI16^{FL}$, 50 μg/mice), or PBS every other day for 6 weeks. They were then euthanized by CO_2 inhalation and skin harvested for further analyses as described later. All treatment groups consisted of 4 mice.

METHOD DETAILS

Reagents, antibodies, and recombinant proteins

CLI-095 was purchased from InvivoGen. Phorbol 12-myristate 13-acetate (PMA) was purchased from Sigma-Aldrich.

The following antibodies were used: rabbit polyclonal anti-IFI16 N-term and C-term (produced as described in[68]), mAb anti-human TLR4 (sc-293072, Santa Cruz Biotechnologies), mAb anti-human TLR4 (sc-13593, Santa Cruz Biotechnologies), mAb anti-β-actin (A1978, Sigma-Aldrich), rabbit IgG-HRP (A6154, Sigma-Aldrich), and mouse IgG-HRP (A16072, Thermo Fisher Scientific).

pET30a expression vectors encoding the human and murine proteins used in this study were purchased from GenScript. All proteins were expressed in ClearColi BL21(DE3) cells (Lucigen) and produced as previously described.[32] The purity of the proteins was assessed by 7.5% or 12% SDS-polyacrylamide gel electrophoresis and revealed by using InstantBlue Coomassie (Expedon) (Figure S5).

Recombinant TLR4/MD2 complex (3146-TM-050/CF) was purchased from R&D Systems.

Cell treatments

For treatments, cells were stimulated in complete medium with equimolar concentration (111 nM) of recombinant proteins for 24 h. For antibody-mediated IFI16 inhibition, increasing concentrations of anti-IFI16 N-term and C-term (1, 5, 10 μg/ml) were preincubated with recombinant IFI16 for 1 h before treatment. For TLR4 inhibition, macrophages were preincubated with CLI-095 (5 μM) for 1 h before treatment.

Sequence alignments, protein structure prediction, docking, and mutagenesis

Sequence alignments of the PYRIN domains were performed using the MEGAX software[71] and the ClustalW algorithm.[72] The primary amino acid sequences were sourced from UniProtKB, designated by the following accession numbers: IFI16 Q16666, MNDA P41218, AIM2 O14862, IFIX Q6K0P9, IFI203 O35368, IFI204 P0DOV2, mAIM2 Q91VJ1, NLRP3 Q96P20, ASC Q9ULZ3, IFI205 Q8CGE8, IFI206 G3UZV2, IFI207 E9Q3L4, IFI208 Q3V3Q4, IFI209 Q8BV49, IFI211 P0DOV1, IFI212 D0QMC3, IFI213 Q3UPZ5, and IFI214 Q504N7. The structural modeling of the of $IFI16^{PYD}$ was performed using Robetta software.[33] Simulations of protein-protein interaction were conducted on the HADDOCK web server,[34] focusing on the potential complexes formed between the N-terminal segment of TLR4 (up to the first 626 amino acids) and the PYD. To ascertain their interaction potential, these complexes were evaluated and ranked according to the HADDOCK score, indicative of a binding free energy-like metric.

The 3D structures of proteins were visualized, binding lengths calculated, and illustrative figures created using PyMOL software (The PyMOL Molecular Graphics System, Version 2.3.4). For site-directed mutagenesis, GenScript was asked to substitute specific residues (*i.e.*, I17, K64, K34, K86, or the combination K64-K34-K86) with alanine or glycine on a pET30a-IFI16 wt or a pET30a-$IFI16^{PYD}$ backbone. The resulting plasmids were then transformed into ClearColi BL21(DE3) cells (Lucigen), where the proteins were expressed and purified following the previously outlined method.

Co-immunoprecipitation and immunoblotting

For co-immunoprecipitation (co-IP) experiments, human macrophages were treated for 1 h with $IFI16^{FL}$, $IFI16^{PYD}$, or left untreated, and whole-cell extracts were prepared using RIPA lysis buffer (Thermo Fisher Scientific) supplemented with protease and phosphatase inhibitor cocktail (Thermo Fisher Scientific). After lysis, co-IP was performed using mAb anti-TLR4 antibody (sc-13593, Santa Cruz Biotechnologies) previously conjugated with magnetic beads (Dynabeads Protein G Immunoprecipitation Kit, ThermoFisher). Co-immunoprecipitated proteins were then separated by electrophoresis using 7.5% or 12% SDS-polyacrylamide gels (Bio-Rad) and transferred to nitrocellulose membranes. After blocking and probing with specific primary and HRP-conjugated secondary antibodies, proteins were detected using ECL (Cyanagen Westar Antares) and images acquired using Quantity One software (version 6.1.0.07, Bio-Rad).

Gene expression analysis

Total RNA was extracted using TRIzol Reagent (Thermo Fisher Scientific) and retrotranscribed using an iScript cDNA Synthesis Kit (Bio-Rad). cDNAs were then analyzed on a CFX96 Real-Time PCR Detection System (Bio-Rad) using SsoAdvanced Universal SYBR Green Supermix (Bio-Rad) and specific primers for *TNFα, IL8, IL1β* and *GAPDH* (housekeeping gene). Gene expression variations were calculated as fold change relative to untreated cells, using the ΔΔCT method. Primer sequences are available upon request.

Cytokine measurement by ELISA

Cytokine production was measured in cell culture supernatants using human IL-8 DuoSet ELISA, human IL-6 DuoSet ELISA, human or mouse TNF-α DuoSet ELISA (all from R&D Systems), ELISA MAX Deluxe Set Human TNF-α, ELISA MAX Deluxe Set Human IL-6 and ELISA MAX Deluxe Set Human IL-1β (all from BioLegend). Absorbance was measured with a Spark multimode microplate reader (Tecan).

Surface plasmon resonance

SPR was performed using the Biacore X100 (Cytiva) instrument as previously described.[32] Briefly, recombinant proteins were flowed over a TLR4/MD2-coated chip, and KDs were calculated using the Biacore evaluation software (Cytiva) assuming a 1:1 binding model. The quality of kinetic constants was validated through specific reliability indicators. To investigate the effect of antibodies on IFI16-receptor binding, increasing concentrations of anti-IFI16 N-term and C-term (62.5, 125, 250, 500 nM) were mixed with 500 nM of recombinant IFI16 for 1 h. These mixtures were then flowed over the TLR4/MD2-coated chip for 120 s and allowed to dissociate for 180 s, and response units (RUs) were recorded. Any background signals from the control flow cell and buffer injections were subtracted from the final RUs.

Flow cytometry

0.5 x 10^6 cells/sample were resuspended in HBSS (Lonza) supplemented with 0.5% BSA (Sigma) and stained for 30 minutes at 4°C with Aqua LIVE/Dead Fixable-405nm staining (Invitrogen, Carlsbad, US) to exclude dead cells, and a mix of antibodies diluted in FACS buffer. The following fluorophore-conjugated antibodies were used: anti-CD11b-A488 (clone M1/70), anti-Ly6C-APC-Cy7 (clone HK1.4), anti-Ly6G-BV711 (clone 1A8), anti F4/80-APC (clone BM8), anti-I-A/I-E-PE (clone M5/114.15.2), anti-CD86-BV650 (clone GL-1), all from Biolegend. After two washes with PBS, cells were acquired with LSRFortessa Cell Analyzer (BD) and analyzed by FlowJo cell analysis software v10.9 (BD).

Skin histology

4-μm thick sections of paraffin-embedded skin tissues were stained with Masson's trichrome staining or toluidine blue staining. Figures were acquired using a Mirax Pannoramic Midi Scanner (3DHISTECH) and analyzed using Slideviewer 2.7 software (3DHISTECH). Dermal thickness was measured as the distance from the epidermis to the subcutaneous tissue. Mast cells were counted in two randomly selected fields of each picture. Measures were performed blinded by two independent researchers.

PI permeabilization assay

The cell death ratio was calculated as previously described.[75] Briefly, differentiated THP-1 cells were incubated or not with CLI-095 for 1h and then treated with $IFI16^{FL}$, recombinant domains or variants, or left untreated. After 24 hours, the cells were washed three times with PBS. Subsequently, 300 μl of a pre-warmed staining solution (containing 5 μM PI, 5% FBS, and 20 mM HEPES in HBSS without phenol red but supplemented with $MgCl_2$ and $CaCl_2$) was added to each well and incubated for 5 minutes at 37°C with 5% CO_2. A 0.1% Triton X-100 solution was used as a positive control to assess maximum permeability. The fluorescence intensity was measured using a Spark multimode microplate reader (Tecan).

Bioinformatics analysis

GEO2R web tool[73] was used to measure the IFI16, TLR4 and TNFA gene expression in 3 publicly available SSc microarray datasets (GSE9285, GSE32413, GSE45485). Patients' stratification was done using a previously published set of "intrinsic" gene signature[68] (https://www.ncbi.nlm.nih.gov/geo/).

QUANTIFICATION AND STATISTICAL ANALYSIS

Statistical differences for comparison between groups were calculated using one-way ANOVA followed by Dunnett's or Sidak's correction for multiple comparison, and considered significant at a *p*-value < 0.05 with levels indicated as: * $p < 0.05$, ** $p < 0.01$, *** $p < 0.001$, **** $p < 0.0001$ and non-significant (ns). Data are express as the mean ± SEM or SD. The number of independent experiments and individual statistical analyses performed can be found in figure legends. Statistical analyses were performed using GraphPad Prism version 9.0.0 for Windows (GraphPad Software, La Jolla California USA, www.graphpad.com).